**Atmospheric
Chemistry
and Physics**

Global atmospheric model for mercury including oxidation by bromine atoms

C. D. Holmes[1], D. J. Jacob[1], E. S. Corbitt[1], J. Mao[1], X. Yang[2], R. Talbot[3], and F. Slemr[4]

[1]Department of Earth and Planetary Sciences and School of Engineering and Applied Sciences, Harvard University, Cambridge, MA, USA
[2]Department of Chemistry, Cambridge University, Cambridge, England
[3]Institute for the Study of Earth, Oceans, and Space, University of New Hampshire, Durham, NH, USA
[4]Max Planck Institute for Chemistry, Air Chemistry Division, Mainz, Germany

Abstract. Global models of atmospheric mercury generally assume that gas-phase OH and ozone are the main oxidants converting Hg^0 to Hg^{II} and thus driving mercury deposition to ecosystems. However, thermodynamic considerations argue against the importance of these reactions. We demonstrate here the viability of atomic bromine (Br) as an alternative Hg^0 oxidant. We conduct a global 3-D simulation with the GEOS-Chem model assuming gas-phase Br to be the sole Hg^0 oxidant (Hg + Br model) and compare to the previous version of the model with OH and ozone as the sole oxidants (Hg + OH/O_3 model). We specify global 3-D Br concentration fields based on our best understanding of tropospheric and stratospheric Br chemistry. In both the Hg + Br and Hg + OH/O_3 models, we add an aqueous photochemical reduction of Hg^{II} in cloud to impose a tropospheric lifetime for mercury of 6.5 months against deposition, as needed to reconcile observed total gaseous mercury (TGM) concentrations with current estimates of anthropogenic emissions. This added reduction would not be necessary in the Hg + Br model if we adjusted the Br oxidation kinetics downward within their range of uncertainty. We find that the Hg + Br and Hg + OH/O_3 models are equally capable of reproducing the spatial distribution of TGM and its seasonal cycle at northern mid-latitudes. The Hg + Br model shows a steeper decline of TGM concentrations from the tropics to southern mid-latitudes. Only the Hg + Br model can reproduce the springtime depletion and summer rebound of TGM observed at polar sites; the snowpack component of GEOS-Chem suggests that 40% of Hg^{II} deposited to snow in the Arctic is transferred to the ocean and land reservoirs, amounting to a net deposition flux to the Arctic of $60 \, Mg \, a^{-1}$. Summertime events of depleted Hg^0 at Antarctic sites due to subsidence are much better simulated by the Hg + Br model. Model comparisons to observed wet deposition fluxes of mercury in the US and Europe show general consistency. However the Hg + Br model does not capture the summer maximum over the southeast US because of low subtropical Br concentrations while the Hg + OH/O_3 model does. Vertical profiles measured from aircraft show a decline of Hg^0 above the tropopause that can be captured by both the Hg + Br and Hg + OH/O_3 models, except in Arctic spring where the observed decline is much steeper than simulated by either model; we speculate that oxidation by Cl species might be responsible. The Hg + Br and Hg + OH/O_3 models yield similar global budgets for the cycling of mercury between the atmosphere and surface reservoirs, but the Hg + Br model results in a much larger fraction of mercury deposited to the Southern Hemisphere oceans.

1 Introduction

Mercury is a neurotoxic pollutant that is dispersed globally by atmospheric transport. Emissions are mostly elemental mercury (Hg^0) and atmospheric observations of Hg^0 imply an atmospheric lifetime on the order of one year (Lindberg et al., 2007). The oxidized product Hg^{II} is highly water soluble and deposits rapidly through precipitation and surface uptake. Understanding the global budget of atmospheric mercury and the source-receptor relationships for mercury deposition therefore requires global atmospheric transport models with accurate redox chemistry.

A fundamental limitation of current models is the uncertainty in the atmospheric chemistry of mercury (Lin et al., 2006; Ariya et al., 2008, 2009). Atmospheric observations imply that oxidation of Hg^0 to Hg^{II} must be photochemical (Shia et al., 1999; Selin et al., 2007). Models generally assume that gas-phase OH and ozone are the main oxidants, and also include aqueous-phase reduction of Hg^{II} to Hg^0 that competes with deposition as a sink for Hg^{II} (Bergan and Rodhe, 2001; Petersen et al., 2001; Cohen et al., 2004; Lin et al., 2006; Seigneur et al., 2006; Selin et al., 2007; Pongprueksa et al., 2008). However, recent work suggests that gas-phase oxidation of Hg^0 by OH and O_3 is too slow to be of atmospheric relevance (Calvert and Lindberg, 2005; Hynes et al., 2009). Heterogeneous oxidation in clouds and aerosols is conceivable but hypothetical (Calvert and Lindberg, 2005; Snider et al., 2008; Ariya et al., 2009). There is also no accepted kinetics or mechanism for Hg^{II} atmospheric reduction (Ariya et al., 2009; Hynes et al., 2009). Present-day measurement techniques cannot determine the molecular identity of atmospheric Hg^{II} oxidation products, but instead quantify all gas-phase Hg^{II} as reactive gaseous mercury (RGM).

Holmes et al. (2006) proposed that gas-phase Br atoms might be the dominant global oxidant of Hg^0, with most of the oxidation taking place in the free troposphere. Several pieces of evidence support this idea. Oxidation of Hg^0 by Br is thought to explain the mercury depletion events (MDEs) in polar spring (Goodsite et al., 2004; Steffen et al., 2008; Xie et al., 2008). Diurnal patterns of Hg^{II} in the marine boundary layer (MBL) are consistent with oxidation by Br (Hedgecock et al., 2005; Holmes et al., 2009). Column measurements suggest a background concentration of 0.5–2 ppt BrO in the free troposphere (Pundt et al., 2002; Van Roozendael et al., 2002; Sinnhuber et al., 2005) that could be accounted for by photolysis and oxidation of bromocarbons (Yang et al., 2005). Br atom concentrations deduced from photochemical equilibrium with this background BrO could yield an Hg^0 atmospheric lifetime of less than a year (Holmes et al., 2006). The lower stratosphere also contains elevated BrO (Salawitch et al., 2005), which might explain the rapid depletion of Hg^0 observed above the tropopause (Talbot et al., 2008).

Constructing a plausible global model of Hg + Br chemistry is challenging because of the large range of reported Hg + Br kinetics (Holmes et al., 2006; Ariya et al., 2008; Hynes et al., 2009) and because of uncertainties in the concentrations of atmospheric Br. Gaseous inorganic bromine (Br_y) originates from atmospheric degradation of bromocarbons and debromination of sea-salt aerosol (von Glasow et al., 2002; Pszenny et al., 2004; Yang et al., 2005). Short-lived bromocarbons are thought to dominate the supply of Br_y in the free troposphere and lower stratosphere; these include $CHBr_3$ and CH_2Br_2 emitted by the ocean and CH_3Br of both biogenic and anthropogenic origin (Yang et al., 2005). Sea salt dominates Br_y supply in the MBL. Br_y cycles between radical forms (Br and BrO) and non-radical reservoir species (HOBr, HBr, $BrNO_3$, $BrNO_2$, and Br_2) (Pszenny

et al., 2004). Br and BrO are in fast photochemical equilibrium during daytime and disappear into the reservoir species at night. Heterogeneous reactions of HOBr, HBr, and $BrNO_3$ on aerosols could also be important for maintaining radical concentrations (von Glasow et al., 2004; Yang et al., 2005). Br_y is eventually removed from the atmosphere by wet and dry deposition.

Three previous global mercury model studies have included Br as an Hg^0 oxidant in addition to OH and O_3 (Ariya et al., 2004; Seigneur and Lohman, 2008; Dastoor et al., 2008). The studies of Ariya et al. (2004) and Dastoor et al. (2008) focused on simulation of Arctic MDEs, where the importance of Br is well established. Seigneur and Lohman (2008) evaluated the sensitivity of the simulated interhemispheric and vertical gradients of Hg^0 to the Hg + Br reaction kinetics. Their simulated mean surface Hg^0 concentrations changed by 20–40% across the range of the kinetic data (Ariya et al., 2002; Donohoue et al., 2006), with the best results obtained with the slow kinetics. In contrast, Dastoor et al. (2008) reported that the fast kinetics gave a better simulation of Hg^0 in the Arctic at Alert, Canada. Seigneur and Lohman (2008) also presented a sensitivity test in which Br was the sole oxidant of Hg^0. This showed an unrealistic peak of Hg^0 in the tropics and minima at the poles.

Here we use the GEOS-Chem global chemical transport model (Selin et al., 2008) to evaluate whether a model with gas-phase Br as the sole Hg^0 oxidant can in fact be consistent with atmospheric observations. The above model studies derived their tropospheric bromine concentrations from satellite observations of BrO columns (Chance, 1998; Burrows et al., 1999), which feature polar maxima of BrO. Recent aircraft observations in the Arctic, however, show that the troposphere contributes less to these polar maxima than previously expected (Salawitch et al., 2010), so earlier models likely overestimated tropospheric Hg^0 oxidation at high latitudes. Here we use a combination of field measurements and process-based models to estimate the distribution of Br from the surface to the stratosphere. We also describe several other recent improvements to the GEOS-Chem mercury model including updated anthropogenic emissions, mechanistic uptake by sea-salt aerosol, scavenging by snow and ice, and a coupled snowpack reservoir. We evaluate the ability of this new model version to reproduce atmospheric observations through comparisons with multiple data sets.

2 Model description

The previous version of the GEOS-Chem atmosphere-ocean-land mercury model (v7.04) was described by Selin et al. (2008). The model includes a global 3-D atmosphere (here $4° \times 5°$ horizontal resolution, 55 vertical levels, hourly time steps) coupled to 2-D surface ocean and soil reservoirs. The atmospheric component is driven by assimilated meteorological data from the Goddard Earth Observing System

(GEOS) of the NASA Global Modeling and Assimilation Office (GMAO). It includes three transported species: Hg^0, Hg^{II}, and inert, nonvolatile particulate mercury (Hg$_P$). The surface ocean component (Strode et al., 2007) includes three species: Hg^0, reactive dissolved Hg^{II}, and inert particle-bound Hg$_P$. These ocean species undergo chemical inter-conversion and vertical exchange with the atmosphere and with a deep ocean reservoir of fixed mercury concentrations. Horizontal transport in the ocean is neglected. Natural soil mercury concentrations are specified on the $4° \times 5°$ grid by steady state of emissions and deposition in the preindustrial atmosphere (Selin et al., 2008). They are augmented for present-day on the basis of the modeled deposition patterns of anthropogenic mercury.

In the present model we have updated the emissions, atmospheric chemistry, and deposition modules used by Selin et al. (2008). We elaborate on these improvements below. We have also updated the transport component by using meteorological input from the GEOS-5 assimilation data, which have $0.5° \times 0.67°$ horizontal resolution and 72 vertical layers. As before, we degrade the resolution to $4° \times 5°$ and 47 layers for computational expediency. Tracer transport algorithms are from the current GEOS-Chem version (8.02.03), which includes improved cross-tropopause transport (MacKenzie, 2009) and a non-local parameterization of boundary layer mixing (Lin and McElroy, 2010). Figure 1 presents our updated global mercury budget, which we will discuss in Sect. 4.

2.1 Emissions

Selin et al. (2008) previously used the GEIA anthropogenic emissions for 2000 (Pacyna et al., 2006) but increased Hg^0 emissions globally by 30% (by 50% in China) to 3400 Mg a^{-1} total Hg in order to accommodate atmospheric observations. Those emissions exceed the 1900–2600 Mg a^{-1} range of recent estimates and are likely too high (Mason and Sheu, 2002; Streets et al., 2009; Pacyna et al., 2010; Pirrone et al., 2010). Here we use the Streets et al. (2009) global inventory for 2006 partitioned into 17 regions; emissions within each region follow the GEIA distribution. In addition, Hg^0 emissions from artisanal gold mining total 450 Mg a^{-1} (Hylander and Meili, 2005; Selin et al., 2008), which is very close to the independent estimate of 400 Mg a^{-1} by Telmer and Veiga (2009). Our anthropogenic emissions thus total 1300 Mg a^{-1} Hg^0, 650 Mg a^{-1} Hg^{II}, and 100 Mg a^{-1} Hg$_P$. While these are 30% lower than in Selin et al. (2008), our simulation remains consistent with the observed Hg^0 concentrations (as we will show below) because changes in the redox chemistry prolong the Hg^0 lifetime.

The soil emissions specified by Selin et al. (2008) were an exponential function of both soil temperature and solar radiation, producing a strong summer peak. With the smaller anthropogenic emissions and slower oxidation in the present model, these emissions would result in a summer Hg^0 max-
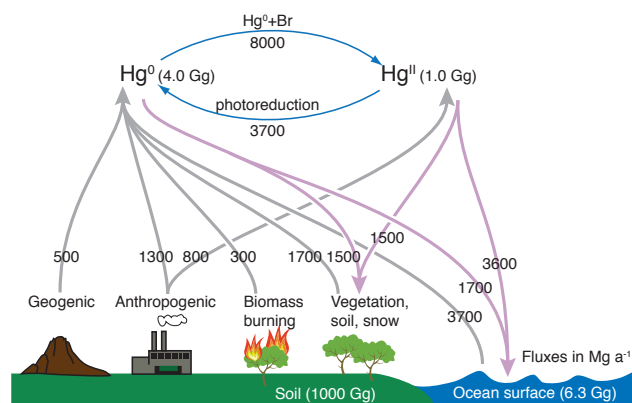

Fig. 1. Global budget of atmospheric mercury derived from this work. Hg^{II} here includes gaseous and particulate forms, plus a negligible contribution (1 Mg) from inert particulate mercury.

imum at northern mid-latitudes that is at odds with observations. Here we specify soil emission E as a function of solar radiation only following Zhang et al. (2001),

$$E = \beta C_s \exp(\alpha R_g), \tag{1}$$

where C_s is the soil mercury concentration (g g^{-1}), R_g is the solar radiation flux at the ground, and $\alpha = 1.1 \times 10^3$ m^2 W^{-1}. The scaling factor $\beta = 0.02$ g m^{-2} h^{-1} is derived here from global mass balance in the preindustrial period, as described by Selin et al. (2008). With this change, simulated Hg^0 concentrations follow the observed seasonal cycle, but total present-day soil emissions, 1200 Mg a^{-1}, are unchanged from Selin et al. (2008).

As in Selin et al. (2008), soil and vegetation emit an additional 260 Mg a^{-1} through rapid photoreduction of deposited Hg^{II}. Biomass burning emits 300 Mg a^{-1} following the distribution of biomass burning CO, using a new Hg/CO emission ratio of 100 nmol mol^{-1} derived in Sect. 3.5. Friedli et al. (2009) estimate larger biomass burning emissions of 675 ± 240 Mg a^{-1} based on satellite-derived fire area and biome-specific emission factors, but our results here are not sensitive to this difference because these emissions are relatively small in any case. The model no longer includes emissions through plant transpiration because of field evidence that this process is unimportant (Gustin et al., 2004).

Arctic field studies find large Hg^0 emissions from sunlit snowpacks in spring and summer, following surface enrichment caused by MDEs (Cobbett et al., 2007; Steffen et al., 2008, and references therein). Some of the mercury deposited during MDEs may be retained in ecosystems during snowmelt (Dommergue et al., 2003; Brooks et al., 2006; Johnson et al., 2008), but low Hg concentrations in late-season snow and meltwater suggest that most of the MDE-deposited mercury returns to the atmosphere (Kirk et al., 2006). We add a snowpack reservoir on the $4° \times 5°$ grid

that accumulates mercury deposition and releases it as Hg^0 under sunlit conditions. The reservoir lifetime is 180 d, decreasing to 21 d when $T > 270$ K to fit observations by Fain et al. (2007, 2008) that re-emission accelerates sharply when melting begins. This simple parameterization reproduces the seasonal cycle of atmospheric Hg^0 at Arctic sites as will be shown in Sect. 3.2. We find that 60% of mercury deposited to snow is eventually reemitted and 40% enters the underlying ocean or soil. Global snow emissions are 210 Mg a^{-1}.

Figure 1 summarizes model emissions. Net ocean Hg^0 emissions respond dynamically to changes in emissions and chemistry and are now 2000 Mg a^{-1}, which is 40% smaller than the earlier model and closer to central estimates from other studies (Lamborg et al., 2002; Mason and Sheu, 2002; Sunderland and Mason, 2007; Mason, 2009). Global mercury emissions are 8300 Mg a^{-1} if we include gross ocean Hg^0 emissions or 6300 Mg a^{-1} if we include only net ocean emission.

2.2 Chemistry

A major update in this work is to oxidize Hg^0 by Br atoms instead of by ozone and OH. Table 1 lists the reactions involved. Atomic bromine initiates Hg^0 oxidation in the gas phase following a mechanism described by Goodsite et al. (2004). The unstable product, HgBr, may either dissociate or react with Br or OH to form Hg^{II}. We use kinetic coefficients from Donohoue et al. (2006), Goodsite et al. (2004) and Balabanov et al. (2005). These coefficients are at the low end of the published range (Holmes et al., 2006) and are similar to the ones chosen by Seigneur and Lohman (2008) to fit observed vertical Hg^0 gradients and by Xie et al. (2008) to model MDEs. OH concentrations for the HgBr + OH → HgBrOH reaction are archived from a GEOS-Chem full-chemistry simulation (Park et al., 2004).

Global bromine concentrations are specified on the model grid by combining estimates of the contributions from major precursors: bromocarbons, halons, and sea-salt aerosol bromide. For the troposphere, except the MBL, and the lower stratosphere we use monthly archived Br from the p-TOMCAT model with biogenic bromocarbon and methyl bromide as the only source gases (Yang et al., 2005). In the middle stratosphere and above, where halons decompose, we use archived Br from the NASA Global Modeling Initiative (GMI) Aura4 model with halon and methyl bromide source gases (Strahan et al., 2007). These model estimates are constrained by observations of the bromocarbon source gases (e.g. Douglass et al., 2004; WMO, 2007; Warwick et al., 2007) and standard gas-phase chemistry of Br_y (Sander et al., 2006). They may be lower limits because we do not account for ventilation of MBL air containing Br_y from sea-salt aerosol (Yang et al., 2005) or heterogeneous reactivation of Br_y on aerosols (von Glasow et al., 2004; Yang et al., 2010).

Sea-salt aerosol bromide is an additional source of Br_y for the MBL. Here we assume a uniform daytime concentration of 1 ppt BrO, consistent with the few observations available (Leser et al., 2003; Saiz-Lopez et al., 2004; Martin et al., 2009; O'Brien et al., 2009) and with the observed diurnal cycle of RGM (Holmes et al., 2009). We calculate the associated Br concentrations from photochemical steady state (Platt and Janssen, 1995),

$$\frac{[Br]}{[BrO]} = \frac{J_{BrO} + k_1[NO]}{k_2[O_3]}, \qquad (2)$$

where J_{BrO} is the BrO photolysis frequency, and $k_1 = 2.1 \times 10^{-11}$ cm^3 molecule^{-1} s^{-1} and $k_2 = 1.2 \times 10^{-12}$ cm^3 molecule^{-1} s^{-1} are the rate coefficients for the BrO + NO → Br + NO$_2$ and Br + O$_3$ → BrO + O$_2$ reactions, respectively (Platt and Janssen, 1995). [NO] = 10 ppt is assumed, and [O$_3$] and mean daytime J_{BrO} are archived from GEOS-Chem full-chemistry simulations (Park et al., 2004; Parrella et al., 2010). We impose a diurnal cycle for Br throughout the atmosphere as done by Holmes et al. (2009) and find that the global model reproduces the observed diurnal cycles of Hg^{II} in the MBL as reported in that earlier study.

Springtime photochemistry of sea salt on sea ice can produce unusually high Br concentrations in the polar boundary layer in spring, resulting in fast oxidation of mercury and ozone (Simpson et al., 2007). BrO concentrations are typically 5–15 ppt (Steffen et al., 2008). Here we specify 10 ppt BrO in the Arctic (Antarctic) boundary layer during March–May (August–October) over areas with sea ice, sunlight, stable conditions, and temperatures below 268 K. We calculate the Br concentration in steady state as above, assuming that O$_3$ is depleted to 2 ppb.

Figure 2 shows the resulting GEOS-Chem Br mixing ratios for the months of January and July. We also show BrO for reference although it does not oxidize Hg^0 in the model. Br and BrO have a strong photochemically driven seasonal cycle in the extratropics. Concentrations increase with altitude due to photochemical production. Minima in the tropical lower troposphere reflect wet deposition of soluble inorganic bromine species. Br concentrations peak at the tropical tropopause due to strong radiation and relatively low ozone, but otherwise show little latitudinal variation in the summer hemisphere. Monthly mean BrO columns range from 1×10^{13} cm^{-2} in the tropics to 4×10^{13} cm^{-2} at the summer pole, which agrees well with values and latitudinal trends observed from satellites (Chance, 1998; Richter et al., 2002; Sioris et al., 2006), after we account for the two-fold difference between 24-h averages shown here and the daytime concentrations detected from space.

From these Br concentration fields and the mechanism in Table 1 we obtain a global Hg^0 chemical lifetime of 6 months, with most of the oxidation taking place in the free troposphere. We find that HgBrOH is the major product, but it and other Hg^{II} species are expected to undergo ion exchange in cloud and aerosol water to produce HgCl$_2$ primarily (Hedgecock and Pirrone, 2001; Lin et al., 2006).

Table 1. Gas-phase mercury-bromine reactions in GEOS-Chem.

Reaction	Rate expression[a]	Reference[b]
$Hg^0 + Br + M \rightarrow HgBr + M$	$1.5 \times 10^{-32}(T/298)^{-1.86}[Hg^0][Br][M]$	(1)
$HgBr \xrightarrow{M} Hg^0 + Br$	$3.9 \times 10^9 \exp(-8357/T)(T/298)^{0.51}[HgBr]$	c
$HgBr + Br \xrightarrow{M} HgBr_2$	$2.5 \times 10^{-10}(T/298)^{-0.57}[HgBr][Br]$	(2)
$HgBr + OH \xrightarrow{M} HgBrOH$	$2.5 \times 10^{-10}(T/298)^{-0.57}[HgBr][OH]$	(2)
$HgBr + Br \rightarrow Hg^0 + Br_2$	$3.9 \times 10^{-11}[HgBr][Br]$	(3)

[a] Rate expressions have units of molecule cm^{-3} s^{-1}. [ ] denotes concentration in units of molecules cm^{-3} and [M] is the number density of air. T is temperature in K.
[b] (1) Donohoue et al. (2006); (2) Goodsite et al. (2004); (3) Balabanov et al. (2005)
[c] Derived from the temperature-dependent reaction free energy ($\Delta G = 56.5$ kJ mol^{-1} at 298 K) for $Hg^0 + Br \rightarrow HgBr$ (Goodsite et al., 2004) and the above rate coefficient for the forward reaction.
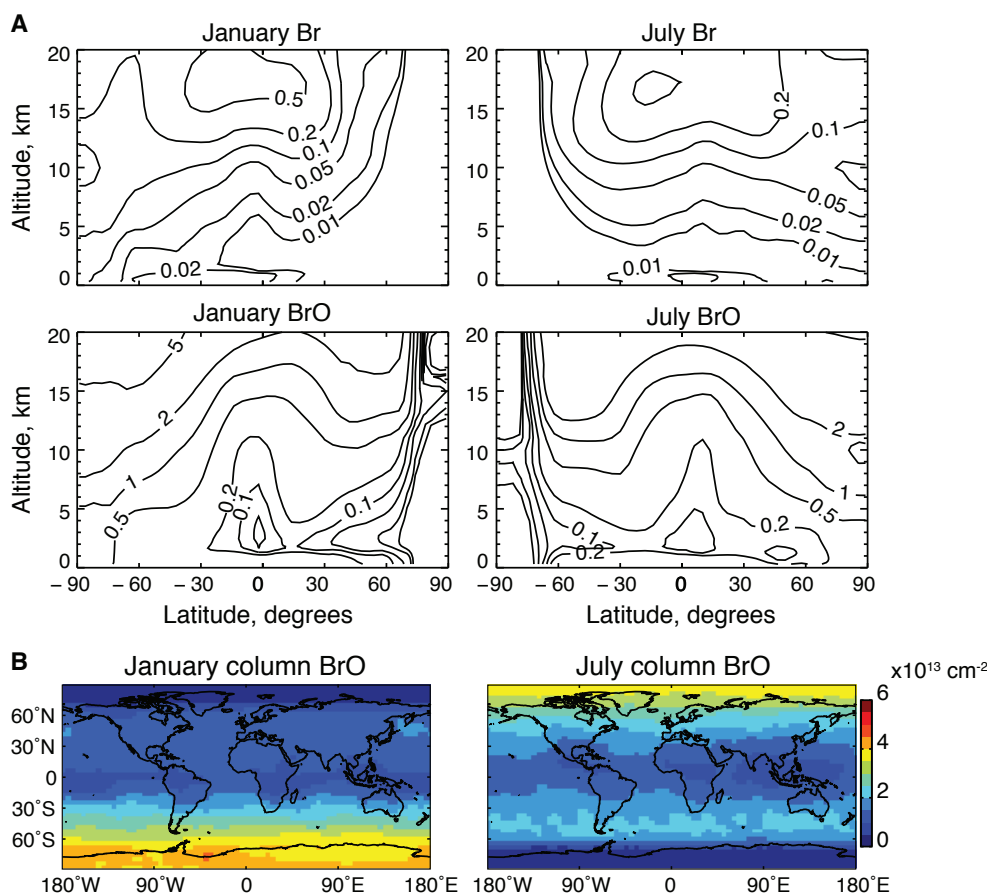
Fig. 2. (A) Zonal mean Br and BrO mixing ratios (ppt) and **(B)** BrO columns for January and July. Values are 24-h averages in GEOS-Chem.

Subsequent deposition of Hg^{II} depends on its gas/aerosol partitioning, for which observations show considerable variability (Jaffe et al., 2005; Caldwell et al., 2006; Liu et al., 2007; Valente et al., 2007; Cobbett et al., 2007; Weiss-Penzias et al., 2009). This partitioning is expected to depend on temperature, aerosol load, and aerosol composition (Lin et al., 2006; Rutter and Schauer, 2007a,b). Future work will link Hg^{II} partitioning to aerosol concentration and composi-

tion in the model, while here we assume 50/50 partitioning of Hg^{II} between the gas and aerosol phase for the purpose of calculating Hg^{II} deposition as described in the following sub-sections.

Our initial simulation without reduction of Hg^{II} produced mean Hg^0 surface concentrations that were smaller than observed. Early global models for mercury included aqueous reduction of Hg^{II} by HO_2 and SO_3^{2-}, but these reactions are
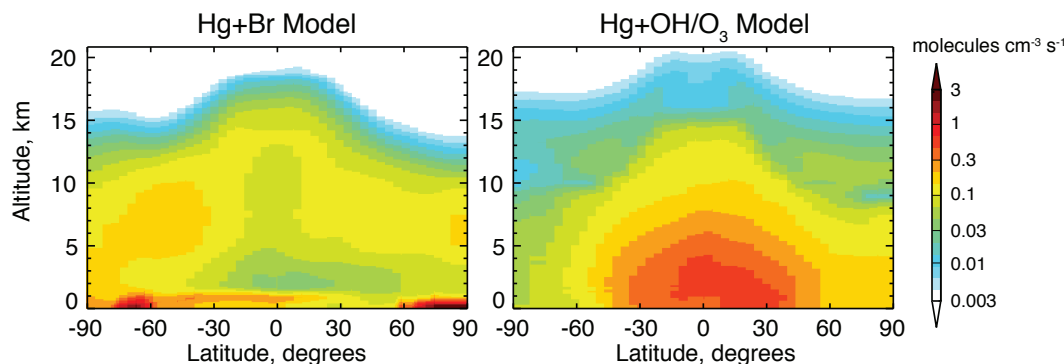
Fig. 3. Annual zonal-mean distribution of the Hg^0 oxidation rate in GEOS-Chem under the Hg + Br and Hg + OH/O$_3$ chemical mechanisms.

now thought to be negligibly slow (Van Loon et al., 2000; Gårdfeldt and Jonsson, 2003). More recent models have hypothesized gaseous or aqueous reactions and tuned the kinetics to match the Hg^0 observations (Selin et al., 2007; Pongprueksa et al., 2008). Laboratory studies have reported fast UV photoreduction of aqueous $HgCl_2$ in the presence of organic acids (Pehkonen and Lin, 1998; Ababneh et al., 2006; Si and Ariya, 2008). We assume Hg^{II} reduction in liquid water clouds to be proportional to the NO_2 photolysis frequency, archived from a GEOS-Chem full-chemistry simulation (J. Mao et al., 2010), and adjust the reduction rate to best match the global mean surface Hg^0 measurements. The best fit yields a Hg^{II} global tropospheric lifetime of 1.7 months against reduction. After including reduction, the mean atmospheric lifetime of mercury is 7.3 months (6.5 months in the troposphere). We will also discuss results from a sensitivity simulation without Hg^{II} reduction and instead decreasing the overall rate of $Hg^0 + Br + X \rightarrow \rightarrow Hg^{II}$ (X $\equiv$ Br, OH) reaction by 60% to yield the same atmospheric lifetime of mercury as in the standard simulation. This decrease in oxidation lies within the range of theory-derived kinetic coefficients for HgBr + X $\rightarrow$ HgBrX (Goodsite et al., 2004; Balabanov et al., 2005) or could be accommodated by lower atomic Br concentrations.

An important objective of this study is to evaluate the ability of GEOS-Chem to fit observations using Br as the sole Hg^0 oxidant instead of OH and ozone. We will compare results from a simulation with Br chemistry (the "Hg + Br model") versus one with OH and ozone chemistry ("Hg + OH/O$_3$ model"). While both oxidation mechanisms, and possibly others, may operate together in the real atmosphere, these idealized simulations enable us to explore the constraints that observations place on the atmospheric chemistry of mercury. For the Hg + OH/O$_3$ model we follow the kinetics of Sommar et al. (2001) and Hall (1995), as used by Selin et al. (2007), with OH and ozone concentrations specified from a full-chemistry GEOS-Chem simulation. The resulting oxidation of Hg^0 is faster than by Br and takes place at lower altitudes where Hg^{II} deposits faster, so we com-

pensate by increasing the reduction rate coefficient 4 fold. The Hg^0 lifetime in that simulation is 3.7 months with OH contributing 80% of the sink, but with the faster reduction the atmospheric lifetime of total mercury is the same as in the Hg + Br model. Figure 3 shows the zonal distribution of Hg^0 oxidation in the Hg + Br and Hg + OH/O$_3$ models. Oxidation by bromine is fast in the MBL where Br number density is largest, but most of the global oxidation occurs in the free troposphere due to low temperatures and increasing Br mixing ratios with altitude (Holmes et al., 2006). Oxidation is also fast in the stratosphere but limited by the small concentrations of Hg^0. The Southern Hemisphere has faster oxidation than the Northern Hemisphere because of the oceanic source of bromocarbons and the low temperatures over Antarctica. Springtime bromine explosions drive secondary oxidation maxima in the polar boundary layers. Oxidation by OH and O$_3$ follows the general distribution of OH concentrations, with a maximum in the lower tropical troposphere and symmetry about the equator. Reduction of Hg^{II} (not shown) peaks at 1–2 km altitude, where cloud liquid water is high, and no reduction occurs above 10 km where clouds are entirely ice.

2.3 Sea-salt aerosol as a sink for mercury

Building on earlier work by Hedgecock and Pirrone (2001) and Selin et al. (2007), we previously suggested that uptake of Hg^{II} by sea-salt aerosol as $HgCl_4^{2-}$ is the dominant sink for Hg^{II} in the MBL and the major source of mercury to the surface ocean (Holmes et al., 2009). We calculated the Hg^{II} uptake rate and subsequent deposition flux (F_{dep}) in a box model of the MBL on the basis of the local 10-m wind speed (u_{10}), relative humidity (saturation ratio S) and mixing depth (H). Fast winds enhance uptake through increased sea spray, while low relative humidity increases [Cl$^-$] within the sea-salt particles and hence promotes formation of $HgCl_4^{2-}$. We accounted for mass-transport limitations at the gas-particle interface over the sea-salt aerosol size distribution. Here we parameterize the results from this MBL box model for
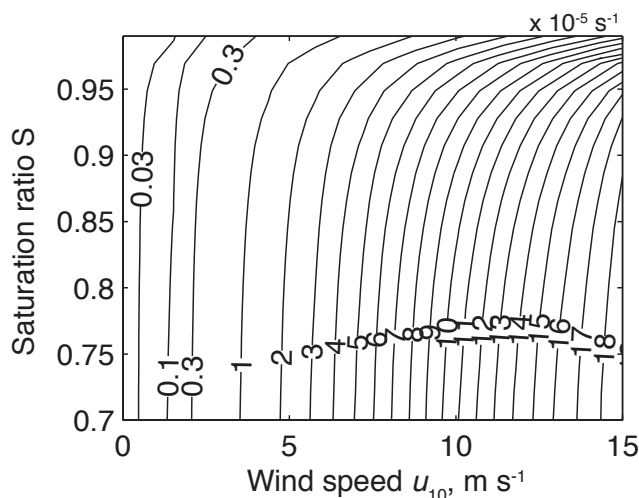
Fig. 4. Rate coefficient k, $(10^{-5}\,\text{s}^{-1})$ for gaseous Hg^{II} uptake and deposition by sea-salt aerosol as simulated by the marine boundary layer model of Holmes et al. (2009) as a function of 10-m wind speed (u_{10}) and water vapor saturation ratio (S). For each (u_{10}, S) pair we conducted 40 Monte Carlo simulations with other box model parameters varying over their likely ranges.

implementation in GEOS-Chem as a first-order rate coefficient (k) for Hg^{II} net uptake and subsequent deposition,

$$F_{\text{dep}} = k(u_{10}, S)\, H\, [\text{Hg}^{\text{II}}], \tag{3}$$

where $[\text{Hg}^{\text{II}}]$ is the MBL concentration. Figure 4 shows $k(u_{10}, S)$ simulated in the box model with full physics over the range of conditions expected in the marine atmosphere (Holmes et al., 2009). We fit k to the following form:

$$k(u_{10}, S) = a_0 \left[1 - \exp(a_1(1-S)) \right] \tag{4}$$
$$\exp\left(a_2\, u_{10} + a_3\, u_{10}^{1/2} + a_4\, u_{10}^{3/2} \right)$$

with coefficients $a_0 = 1 \times 10^{-10}\,\text{s}^{-1}$, $a_1 = -59.91$, $a_2 = -1.935\,\text{s}\,\text{m}^{-1}$, $a_3 = 9.009\,\text{s}^{1/2}\,\text{m}^{-1/2}$, and $a_4 = 0.1477\,\text{s}^{3/2}\,\text{m}^{-3/2}$. This simplified model closely fits the 24-h mean loss rate in the full-physics model ($r^2 = 0.97$) over the parameter range $0.7 \leq S \leq 0.99$ and $0.1 \leq u_{10} \leq 20\,\text{m}\,\text{s}^{-1}$.

2.4 Other deposition processes

GEOS-Chem includes wet scavenging of Hg^{II} and Hg_{P} following the scheme of Liu et al. (2001), and dry deposition of Hg^0, Hg^{II}, and Hg_{P} following the resistance-in-series scheme of Wesely (1989). Selin and Jacob (2008) describe how these schemes apply to mercury in the previous version of the model. They assumed Hg^{II} to be gaseous HgCl_2 for the purpose of computing deposition; the Henry's law solubility constant of HgCl_2 is $1.4 \times 10^6\,\text{M}\,\text{atm}^{-1}$ (Lindqvist and Rodhe, 1985), sufficiently high for near-100% scavenging

in clouds and fast dry deposition limited by aerodynamic resistance. Here we assume 50/50 partitioning of Hg^{II} between the gas and aerosol phase, which increases the lifetime of Hg^{II} against dry deposition as compared to the previous model version.

Selin and Jacob (2008) assumed no scavenging of Hg^{II} in cold (frozen) clouds and snow, and zero retention efficiency of Hg^{II} upon cloud freezing, in order to reproduce the observations of low wet deposition fluxes of mercury at northern US sites in winter. However, observations by Douglas et al. (2008) indicate high mercury concentrations in rime ice, implying high retention efficiency. Therefore we now assume that supercooled water in mixed-phase clouds retains all Hg^{II} and Hg_{P} during freezing. Douglas et al. (2008) and Johnson et al. (2008) found by contrast very low Hg concentrations in ice grown from the vapor phase, so we still assume no mercury scavenging by cloud ice. Below-cloud scavenging by snow is included only for aerosol Hg^{II} and Hg_{P}, with the same efficiency as by rain (Murakami et al., 1983; Feng, 2009). Sigler et al. (2009) found that snowfall has little effect on ambient RGM, so we do not include below-cloud scavenging of gaseous Hg^{II} by snow. Adding low-temperature scavenging as described above increases deposition at high latitudes, but also allows low-latitude convective rainfall to scavenge from higher altitudes.

3 Model evaluation

We test here whether the Hg + Br model (simulation with Hg^0 oxidation initiated by Br only) can reproduce the general patterns seen in atmospheric observations, and compare these results to the Hg + OH/O_3 model (simulation with Hg^0 oxidation by OH and O_3). All simulations are initialized over 15 years of repeated present-day meteorological data to reach annual steady state in the stratosphere. We then analyze model results averaged over 2006–2008 and compare to observed air concentrations and wet deposition fluxes.

3.1 Global distribution of mercury

Figure 5 shows annual mean observed surface concentrations of total gaseous mercury (TGM $\equiv \text{Hg}^0 + $ RGM) compared to the Hg + Br model. TGM in the model is calculated as $\text{Hg}^0 + 0.5\,\text{Hg}^{\text{II}}$. The measurements include annual means at 39 land sites during 2000–2008, plus data from ship cruises (Lamborg et al., 1999; Laurier et al., 2003; Temme et al., 2003; Laurier and Mason, 2007; Soerensen et al., 2010a). Trends in mean TGM during the last decade are small (of order 1% a^{-1}) or negligible at most background sites in the Northern Hemisphere (Temme et al., 2007; Wangberg et al., 2007). Southern Hemisphere data contain larger trends (Slemr et al., 2010) which we discuss below. The model reproduces the spatial variability observed at at the 39 land sites ($r^2 = 0.81$). The mean and
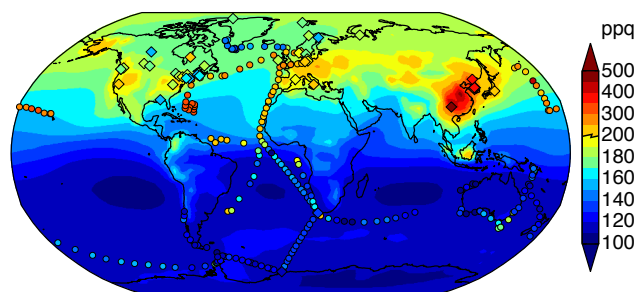
Fig. 5. Global distribution of total gaseous mercury (TGM) concentrations in surface air (1 ppq $= 10^{-15}$ mol mol^{-1} $= 8.97$ pg m^{-3} at 273 K, 1013 hPa). Model values (background) are annual means for 2006–2008. Data for land sites (diamonds) are annual means for available years during 2000–2008 and all other observations from ship cruises (circles) are averaged over 1° latitude bins. Observations include those used by Selin et al. (2007), plus additional sites in Europe (Steffen et al., 2005, EMEP 2009), North America (Steffen et al., 2005; Yatavelli et al., 2006; Stamenkovic et al., 2007; Temme et al., 2007; Choi et al., 2008; Sigler et al., 2009, E. Edgerton, personal communication, 2008), East Asia (Nguyen et al., 2007; Sakata and Asakura, 2007; Feng et al., 2008; Wan et al., 2009), South Africa (Slemr et al., 2010) and the Galathea cruise (Soerensen et al., 2010a). Note the change in linear color scale at 200 ppq.

standard deviation for the ensemble of sites is 209 ± 112 ppq (1 ppq $= 10^{-15}$ mol mol^{-1} $= 8.97$ pg m^{-3} at 273 K, 1013 hPa) in the observations and 191 ± 59 ppq in the model. The model is unbiased with respect to sites in Europe and North America. The Hg + OH/O$_3$ model matches observations similarly well (189 ± 56 ppq, $r^2 = 0.80$) because anthropogenic emissions strongly influence the variability of TGM concentrations at the land sites.

A prominent deficiency in the model, previously identified by Selin et al. (2007), is that it does not reproduce the high concentrations observed over the North Atlantic and Pacific Oceans during ship cruises. This is likely due to upwelling mercury from the sub-surface ocean, possibly reflecting the legacy of past anthropogenic emissions. Although this is not captured in our simulation, where uniform sub-surface ocean mercury concentrations are assumed globally (Strode et al., 2007), Soerensen et al. (2010b) find that forcing GEOS-Chem with observed sub-surface North Atlantic concentrations can reproduce the high atmospheric concentrations observed over the North Atlantic. This will be implemented in a future version of the model.

Figure 6 shows that the Hg + Br and Hg + OH/O$_3$ models diverge in their surface TGM predictions for the Southern Hemisphere because of the different oxidant distributions (Figs. 2 and 3). The Hg + Br model predicts 110–120 ppq TGM at southern mid-latitudes vs. 140–150 ppq in the Hg + OH/O$_3$ model. The Hg + Br model better simulates land stations in Antarctica (Temme et al., 2003) and
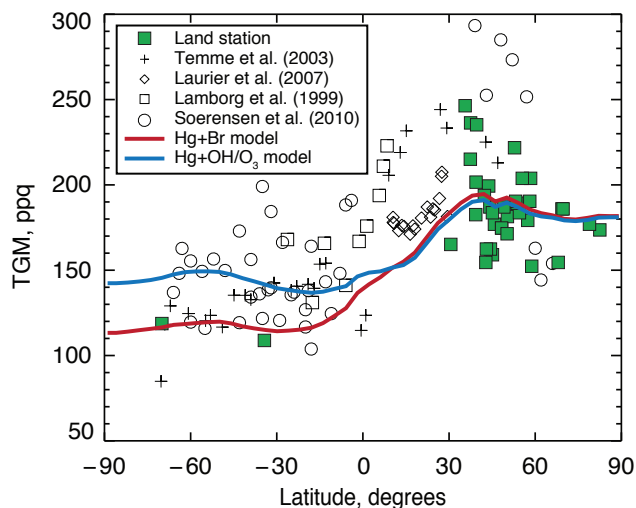

Fig. 6. Meridional gradient of total gaseous mercury (TGM). The model is averaged zonally during 2006–2008. Observations are the same as in Fig. 5.

Cape Point, South Africa (F. Slemr, unpublished post-2008 data). However the trend at Cape Point from 135 ppq during 2000–2004 to 105 ppq after 2008 (Slemr et al., 2010) spans the range between the Hg + Br and Hg + OH/O$_3$ models. Ship data at southern mid-latitudes likewise encompass a wide range (110–160 ppq), likely caused by variability in marine emissions, that does not discriminate between the two simulations. Additional long-term measurements at a southern mid-latitude site, complementing the record at Cape Point, together with greater constraints on Southern Hemisphere ocean emissions would further test the Hg^0 oxidation mechanism.

The meridional gradient in Fig. 6 differs markedly from the model of Seigneur and Lohman (2008), which predicted peak Hg^0 in the tropics and unrealistically low concentrations in the extra-tropics when Br was the sole oxidant. Seigneur and Lohman inferred Br concentrations from the GOME BrO columns, imposing vertical distributions and Br/BrO ratios from the p-TOMCAT CTM (Yang et al., 2005). That CTM does not include halons and would therefore greatly underestimate the contribution of the stratosphere to the BrO column. Considering that the stratospheric contribution is what causes the BrO column increase with latitude (Fig. 2), this method would particularly overestimate tropospheric Br and, hence, Hg^0 oxidation at high latitudes.

3.2 Seasonal cycle at surface sites

Figure 7 compares simulated and observed seasonal cycles of TGM at surface sites. Northern mid-latitude sites show on average a late summer minimum in both observations and the model. Bergan and Rodhe (2001) and Selin et al. (2007)
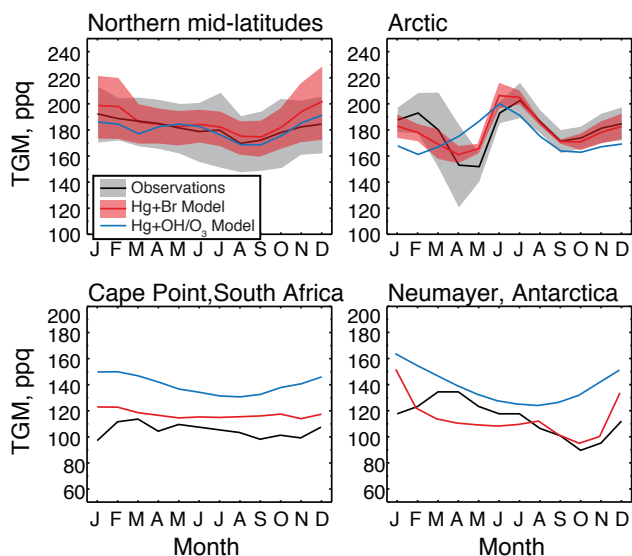
Fig. 7. Mean seasonal variation of total gaseous mercury (TGM) at Arctic, northern mid-latitude, and Southern Hemisphere sites. The northern mid-latitude panel shows an average over 15 sites where monthly mean data are available, including the sites from Selin et al. (2007) plus Andoya and Birkenes, Norway (EMEP 2009); Kuujjuarapik, Canada (Steffen et al., 2005); Athens, Ohio; and Pensacola, Florida in the US (Yatavelli et al., 2006, E. Edgerton, personal communication, 2008). Cape Point data are means for 2007–2008 (F. Slemr, unpublished data). The Arctic panel is an average over 3 sites: Alert, Canada; Zeppelin, Norway; and Amderma, Russia (Steffen et al., 2005, EMEP 2009). Shaded areas show standard deviation among sites for observations and for the Hg + Br model.

attributed this seasonal cycle to the photochemical sink from OH, and we obtain the same result with oxidation by Br which also peaks in summer.

At Cape Point, the only site with long-term data in the Southern Hemisphere outside Antarctica, TGM displays little seasonal variation during recent years, as shown. Before 2004, however, TGM had larger variation with TGM maxima in summer (December–February), in contrast to the Northern Hemisphere (Slemr et al., 2008). The Hg + OH/O$_3$ model reproduces the earlier pattern, which reflects the maximum of ocean emissions in austral summer caused by biological and photochemical reduction of aqueous Hg^{II} (Strode et al., 2007; Slemr et al., 2008). The Hg + Br model has smaller seasonal variation due to the offsetting effect of strong oxidation by Br at southern mid-latitudes in summer and this coincides with the recent seasonal data. This reinforces the value of additional measurements of mercury concentration and interannual variability of ocean fluxes in Southern Hemisphere.

Observations at Arctic sites and at the Neumayer Antarctic site show a springtime minimum driven by MDEs and a summertime maximum driven by re-emission from the snowpack (Steffen et al., 2005; Cobbett et al., 2007). The Hg + Br model can reproduce this seasonal variation but not the Hg + OH/O$_3$ model, which does not include MDEs. We find that atmospheric concentrations are consistent with re-emission of 60% of Hg deposited to the snowpack during springtime and 40% net incorporation into the ocean and soil. The area within the Arctic Circle receives 60 Mg a^{-1} net deposition in the Hg + Br model vs. 40 Mg a^{-1} in the Hg + OH/O$_3$ model without MDEs. The Antarctic Circle similarly receives 70 Mg a^{-1} in the Hg + Br model, but only 20 Mg a^{-1} in the Hg + OH/O$_3$ model. Dastoor et al. (2008) estimate a similar re-emission fraction from snow, but 3 times larger net deposition to the Arctic surface.

3.3 Testing oxidation chemistry through Antarctic subsidence events

Observations at Antarctic sites show frequent summertime events of depleted Hg^0 and enhanced RGM together with elevated ozone (Sprovieri et al., 2002; Temme et al., 2003; Aspmo and Berg, 2009). These differ from springtime depletion events in that O$_3$ is anti-correlated with Hg^0. From four events in the published Neumayer and Terra Nova Bay data (Sprovieri et al., 2002; Temme et al., 2003), we estimate ranges of −6.0 to −11.5 for ΔHg^0/ΔO$_3$ and 1.5 to 4.0 for ΔRGM/ΔO$_3$. Aspmo and Berg (2009) used back-trajectories to identify the mid-troposphere as the source region for such events. Brooks et al. (2008) also found that subsiding air at the South Pole contains elevated Hg^{II}. These observations provide a sensitive test for Hg^0 oxidation chemistry in the model because the cold, dry Antarctic atmosphere minimizes the confounding effect of aqueous reduction. In addition, Br is an effective Hg^0 oxidant over Antarctica in summer (Fig. 3) while OH is ineffective.

Figure 8 shows simulated Hg^0 and RGM at Neumayer for January 2008, and O$_3$ from a GEOS-Chem full-chemistry simulation at the same time and location (J. Mao et al., 2010). The model time series shows several subsidence events with enhanced O$_3$ and RGM, and depleted Hg^0. These events last 1–3 days, as found by Temme et al. (2003). We derive the model ΔHg^0/ΔO$_3$ and ΔRGM/ΔO$_3$ ratios shown in Fig. 8B from a reduced major-axis fit to the January time series. The ratios in the Hg + Br model are consistent with observations while those in the Hg + OH/O$_3$ model are much too weak.

3.4 Wet deposition

Figure 9 compares the Hg + Br model with annual wet deposition measurements from the Mercury Deposition Network (MDN, National Atmospheric Deposition Program, 2009) over North America and the European Monitoring and
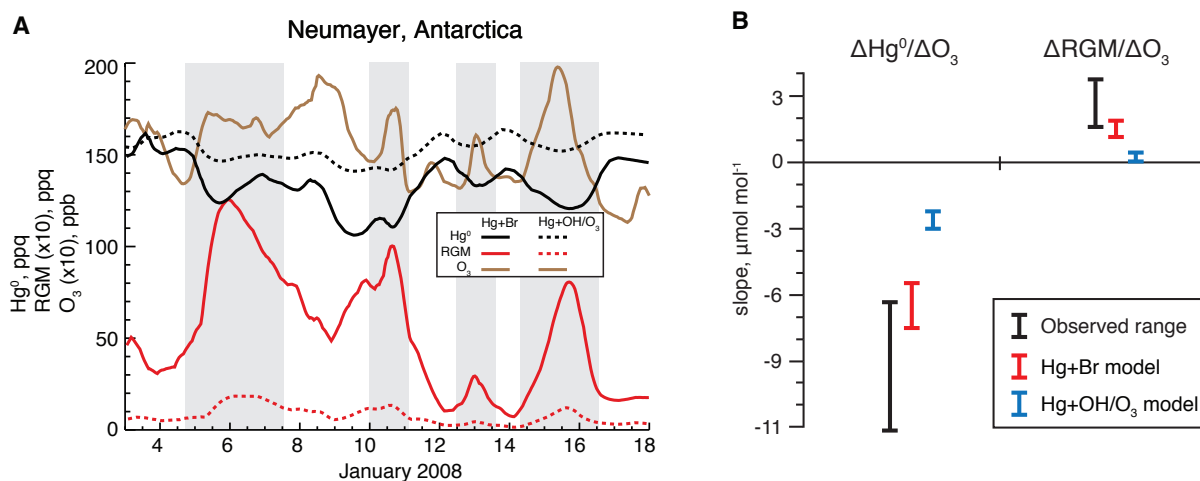
Fig. 8. **(A)** Time series of Hg^0, RGM and O$_3$ simulated at Neumayer, Antarctica in the Hg + Br and Hg + OH/O$_3$ models. Shaded regions show summertime subsidence events diagnosed with relative humidity and O$_3$ data. **(B)** ΔHg^0/ΔO$_3$ and ΔRGM/ΔO$_3$ ratios during January–February. Observed ratios were calculated from data reported by Temme et al. (2003). Modeled ranges are 95% confidence intervals for the reduced major-axis slope from the bootstrap method.
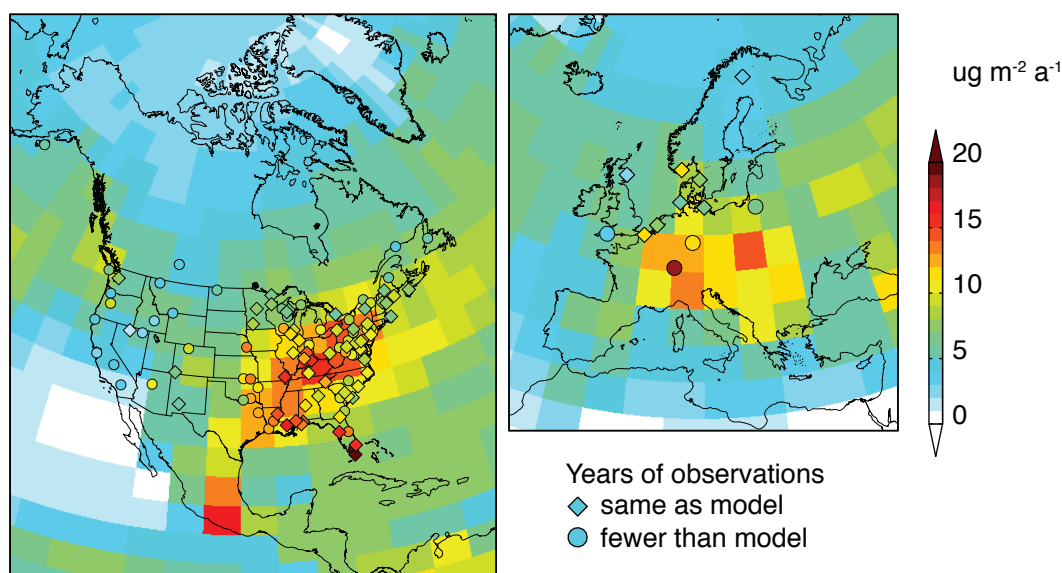

Fig. 9. Annual mercury wet deposition over North America during 2006–2008 and Europe during 2006–2007 from the Hg + Br model. Overlaid points show observations for the same years from the Mercury Deposition Network (MDN) over North America and from the European Monitoring and Evaluation Programme (EMEP) over Europe.

Evaluation Programme (EMEP) over Europe. These networks collect weekly (MDN) or monthly (EMEP) integrated samples. We use sites with at least 75% of annual data available for the simulated years, 2006–2008. We also require fewer than 5 consecutive missing samples for MDN. Both MDN and EMEP have been used extensively to test atmospheric mercury models (e.g. Selin and Jacob, 2008; Bullock et al., 2009; Gusev et al., 2009) and to evaluate the impact of mercury emission reductions (e.g. Butler et al., 2008; Wangberg et al., 2007; Pacyna et al., 2009; Prestbo and Gay, 2009).

Wet deposition is very similar in the Hg + OH/O$_3$ model except where discussed below.

The model predicts the highest wet deposition in the coal-burning regions of Europe and North America, reflecting near-field deposition of Hg^{II} and Hg$_P$ emissions. Observations over Europe are elevated in the industrialized central region and show a poleward decrease in deposition with similar magnitude to the model. Over the Eastern US, the observations likewise show high deposition stretching from Texas to the Mid-Atlantic states, where anthropogenic

mercury emissions are largest. At the northern end of this band the model exceeds observations, regardless of oxidant.

Figure 10 shows the seasonal cycle of wet deposition in the Eastern US and reveals that the positive model bias in the Northeast occurs mainly in winter. Suppressing cold scavenging can eliminate the bias, as found by Selin and Jacob (2008), but observations indicate that such scavenging occurs (Douglas et al., 2008), and suppressing cold scavenging in the model would cause 40% underestimates of deposition in Alaska, Alberta and Finland. Fast reduction may compete with near-field deposition for the fate of Hg^{II} emissions. We assume in the model that reduction is photochemical and therefore ineffective in winter, but it is possible that reduction occurs in all seasons or, equivalently, that the fraction of mercury emitted as Hg^{II} is too high in current inventories (Edgerton et al., 2006; Pongprueksa et al., 2008). This would decrease wet deposition over the Mid-Atlantic and Midwest emission regions (Lohman et al., 2006; Vijayaraghavan et al., 2008).

Sites around the Gulf of Mexico report the highest mercury wet deposition in North America, even though regional mercury emissions are lower than in the Northeast US. Convective scavenging of mercury from the free troposphere likely causes this regional feature (Guentzel et al., 2001; Selin and Jacob, 2008). The Hg + Br model underpredicts wet deposition here by 50%. While the Hg + OH/O_3 model is closer to observations in the northern Gulf region, it is still 40% lower than MDN sites in southern Florida. On a monthly basis, both models overlap the observed wet deposition range in the Gulf region during November-May, as seen in Fig. 10, but only the Hg + OH/O_3 model has a strong deposition peak during the wet summer months, which accounts for its better comparison with the annual mean. During these months OH provides a vigorous subtropical Hg^{II} source available for convective scavenging in the Hg + OH/O_3 model, while there is little Br present in the Hg + Br model. Br concentrations could be larger than are specified here if ventilation of sea-salt-derived Br_y from the MBL or heterogeneous reactivation of Br_y are important (see Sect. 2.2).

3.5 Aircraft measurements

Figure 11 shows mean vertical profiles measured from aircraft during the INTEX-B and ARCTAS campaigns over North America and the Pacific and Arctic Oceans (Talbot et al., 2007, 2008; H. Mao et al., 2010), plus CARIBIC flights over the Atlantic Ocean, Eurasia and North America (Ebinghaus et al., 2007; Slemr et al., 2009). Due to uncertain inlet loss of RGM, the measurements include Hg^0 plus some fraction of gaseous Hg^{II}. This provides an upper limit for Hg^0 and a lower limit for TGM, and we refer to it here as Hg^{0*}. We increase the INTEX-B measurements by 40% based on an in-flight intercomparison (Swartzendruber et al., 2008). The aircraft data are still ~10% lower on average than the
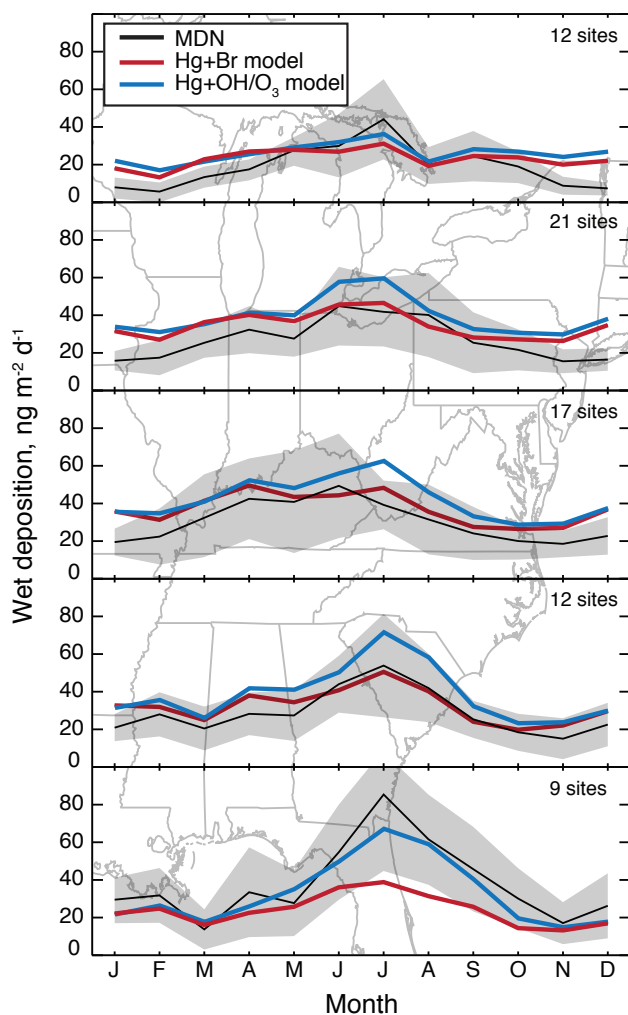

Fig. 10. Mean seasonal variation of mercury wet deposition to the Eastern United States for 2006–2008. Observations include all MDN sites within each depicted region with more than 21 days of data per month; black lines are means with ± standard deviations shaded. Insets list the number of MDN sites. Model results are averaged over each of the 4° × 20° regions shown.

model, but we focus this analysis on the shape of the vertical profile rather than the absolute values, since the model is unbiased relative to observations at surface sites (Sect. 3.1). CARIBIC and ARCTAS observations here exclude biomass burning plumes (CO > 200 ppb or CH_3CN > 0.25 ppt) because the model uses monthly climatological fire emissions.

The observations show boundary layer enhancements over Mexico and the subtropical Pacific Ocean, indicative of surface emissions, and ubiquitous MDEs in the Arctic boundary layer in spring (H. Mao et al., 2010). The model is consistent with these features. Otherwise the concentrations are uniform with altitude in the troposphere, both in the model and the observations, reflecting the long atmospheric lifetime of
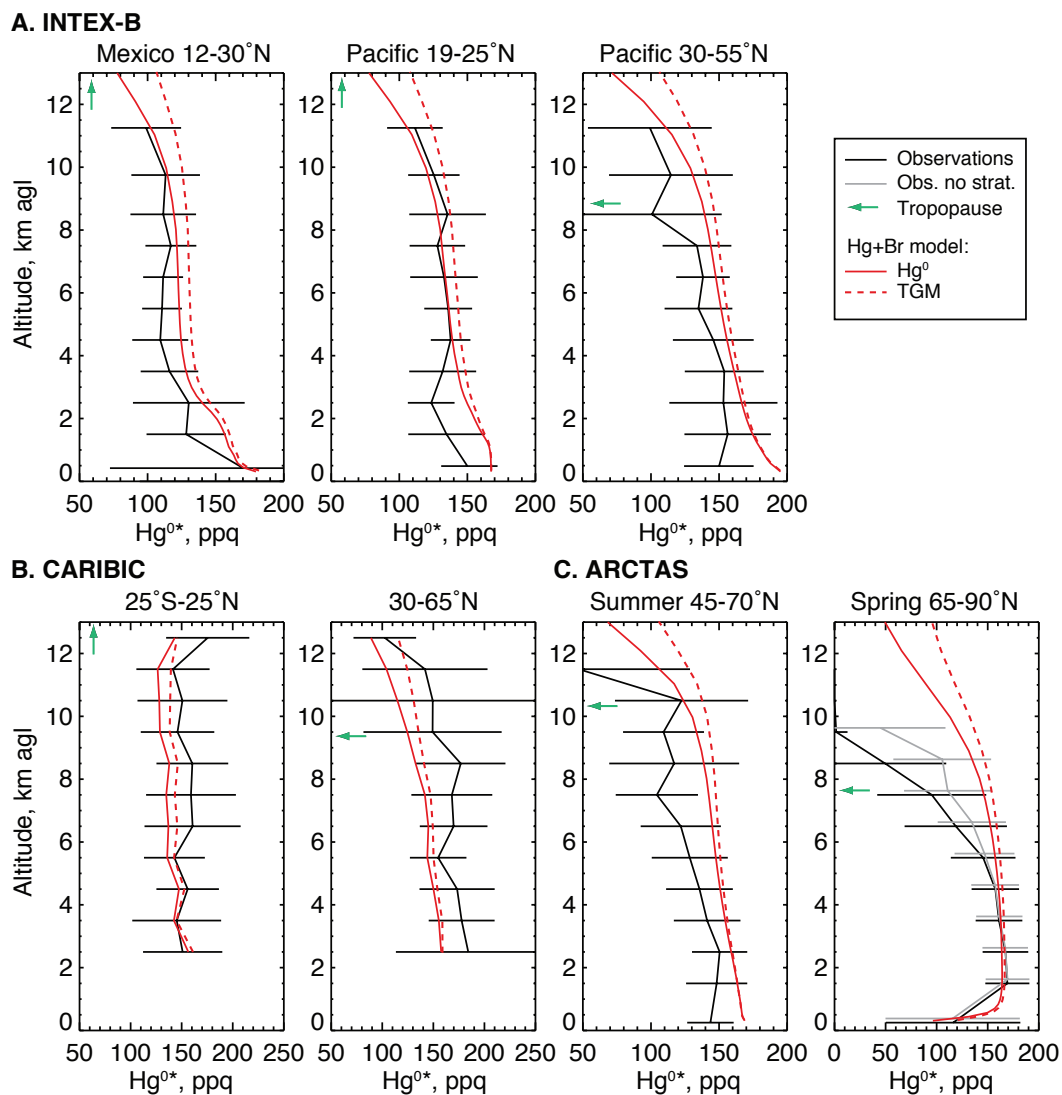
Fig. 11. Mean vertical profiles and standard deviations of mercury concentrations measured by aircraft and compared to the Hg + Br model. **(A)** INTEX-B over Mexico during March 2006 and over the North Pacific Ocean during April–May 2006 (Talbot et al., 2008; Singh et al., 2009). We correct a low bias of 40% in the observations based on an in-flight intercomparison (Swartzendruber et al., 2008). **(B)** CARIBIC flights over Europe, Asia, Africa, and the Atlantic Ocean during 2005–2008 (Slemr et al., 2009). **(C)** ARCTAS flights over North America and the Arctic Ocean in summer 2008 (45–70° N) and spring 2008 (65–90° N) (H. Mao et al., 2010). Arrows show observed mean tropopause $(O_3 = 100 \, ppb)$. Gray lines in the lower right panel show data for troposphere only. Model results show Hg^0 and TGM monthly mean mixing ratios over each flight region (INTEX-B and ARCTAS) or instantaneous values along the flight track (CARIBIC). Altitudes are above ground level. Note the different horizontal scales. See text for definition of Hg^{0*}.

Hg^0. Of most interest here is the observed decline of concentrations above the tropopause. This decline is generally reproduced in the model if we assume that measurements quantify Hg^0 only (or equivalently that Hg^{II} is present mainly in the aerosol). Vertical gradients across and above the tropopause are similar in the Hg + Br and Hg + OH/O$_3$ simulations, and so do not provide an effective test of the chemical mechanism.

One prominent discrepancy is the inability of the model to simulate the steep decline above the tropopause in the Arctic springtime. Complete Hg^{0*} depletions were common during ARCTAS in stratospheric air with O$_3$ > 100 ppb, and Hg^{0*} was rarely detectable when O$_3$ exceeded 200 ppb, suggesting that oxidation increases abruptly above the tropopause (Talbot et al., 2007; Kim et al., 2009). We tested whether additional Br could be responsible by doubling it in the model throughout the stratosphere, corresponding to 4 ppt BrO in

the lowermost stratosphere. Simulated Hg^0 decreased by only 10 ppq at 10 km. Much higher bromine concentrations are unlikely based on satellite observations (Chance, 1998) and constraints on the stratospheric bromine budget (Liang et al., 2010; Salawitch et al., 2010). In another sensitivity test, we added Hg^0 oxidation by BrO to the model (Raofie and Ariya, 2004), but this reaction enhanced Hg^0 oxidation throughout the column rather than specifically in the stratosphere.

Additional oxidants in the springtime polar stratosphere might include Cl, Cl_2, and BrCl generated by heterogeneous chemistry. Hg^0 oxidation reactions with these species are fast (Ariya et al., 2002; Donohoue et al., 2005) but limited by the low oxidant concentrations. The GMI Aura model predicts mean values of ∼1 ppt ClO in the lowermost stratosphere during spring ARCTAS, corresponding to 0.5 ppq Cl and up to 100 ppt Cl_2 and 30 ppt BrCl (Strahan et al., 2007). Based on the available kinetic data (mainly 298 K), the resulting lifetime of Hg^0 exceeds 1 year, too long to account for Hg^0 depletion. However, Thornton et al. (2003) observed much greater chlorine activation (∼10 ppt ClO) in the Arctic winter stratosphere than predicted by the GMI model. At these levels, Cl, Cl_2 and BrCl could become important Hg^0 oxidants.

The ARCTAS flights over California and Nevada (Jacob et al., 2010) provided a first opportunity for detailed boundary layer mapping of a continental source region (Fig. 12). Polluted conditions during these flights caused intermittent low bias in one of the two instrument channels, which we correct by removing the lower value of each consecutive measurement pair. The highest concentrations were in biomass burning plumes sampled in both northern and southern California. The three most concentrated plumes had Hg/CO enhancement ratios of 90–130 nmol mol^{-1} and the mean enhancement ratio for all fire plumes (identified by $CH_3CN > 0.25$ ppt) was 80 nmol mol^{-1}. Weiss-Penzias et al. (2007) and Finley et al. (2009) found similar Hg/CO enhancements (136 ± 60 nmol mol^{-1}) in the Pacific Northwest during summers 2004–2005, and Talbot and Mao (2009) found 60 nmol mol^{-1} during summer ARCTAS flights over Canada, which are similar to ratios of 70–240 nmol mol^{-1} observed worldwide (Ebinghaus et al., 2007; Friedli et al., 2009). Based on these measurements, we reduced the Hg/CO emission ratio for biomass burning in GEOS-Chem to 100 nmol mol^{-1} in this work (previously 210 nmol mol^{-1}), as discussed in Sect. 2.1.

Apart from the fire plumes, the California observations show highest Hg^{0*} near industry and ports in Los Angeles and Long Beach. Typical concentrations exceeded 200 ppq throughout the Los Angeles basin, following a pattern that closely resembles the emission distribution in the EPA source inventory (EPA, 2008). A fresh anthropogenic plume with high SO_2 encountered near the Mexican border does not correspond with any nearby sources in the inventory, suggesting that some industrial emissions in the border region
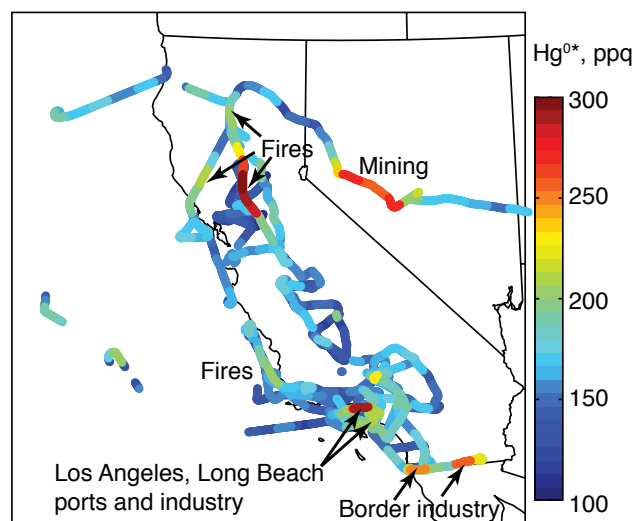

Fig. 12. Mercury distribution in the boundary layer (<2 km a.g.l.) during ARCTAS flights over California and Nevada (June 2008). Sources are identified through correlations with other species (CO, O_3, CH_3CN, HCN).

are underestimated. Offshore marine airmasses contained up to 200 ppq Hg^{0*} as well as elevated dimethyl sulfide indicative of ocean emissions. Mercury levels also persisted above 220 ppq for 150 km on a flight over active and inactive mines in western Nevada. These elevated concentrations are typical for summertime at surface sites in Nevada and may result from a mix of mining operations and naturally Hg-enriched soils (Lyman and Gustin, 2008).

3.6 Is atmospheric reduction necessary to explain observations?

Global models of atmospheric mercury require atmospheric reduction of 4000–10000 Mg a^{-1} Hg^{II} to achieve an unbiased simulation of mean TGM observations with current emission inventories (Bergan and Rodhe, 2001; Lin et al., 2006; Seigneur et al., 2006; Selin et al., 2007, this work). While several reductants for Hg^{II} have possible atmospheric relevance (see review by Ariya et al., 2008), atmospheric importance has not been established for any; so the role of Hg^{II} reduction in the global atmosphere remains conjectural (Hynes et al., 2009). Fast reduction may occur in fresh power plant plumes (Edgerton et al., 2006; Landis et al., 2009), but the global effect would be small because the anthropogenic Hg^{II} source is only 700 Mg a^{-1}. We find in our Hg + Br model that all simulation results can be replicated without atmospheric reduction if we decrease the overall rate of Hg^0 conversion to Hg^{II} by 60%. This could be accommodated within the range of theory-derived kinetic coefficients for the reaction HgBr + X → HgBrX (X ≡ Br, OH) (Goodsite et al., 2004; Balabanov et al., 2005) or by smaller Br concentrations. Until better constraints on Hg^0 oxidation rates

are available, it appears that atmospheric reduction is not required to explain any of the major features of the global mercury cycle.

4 Global mercury budget

Figure 1 shows the global atmospheric mercury budget derived from our $Hg + Br$ simulation in GEOS-Chem. Emissions and deposition in our $Hg + OH/O_3$ simulation differ from the figure by less than 10%. The troposphere accounts for 99% of total atmospheric Hg^0 but only 50% of Hg^{II}, reflecting the lack of Hg^{II} chemical or depositional loss in the stratosphere. The Hg^{II} burden in Fig. 1 includes inert particulate mercury Hg_P but it contributes only 2 Mg. Nearly all redox fluxes occur in the troposphere, as seen in Fig. 3.

Anthropogenic emissions here are 2050 Mg a^{-1} and total emissions are 8300 Mg a^{-1}, both within the literature range as described in Sect. 2.1. Although the original GEOS-Chem model of Selin et al. (2007) used similar anthropogenic emissions (2200 Mg a^{-1}), Selin et al. (2008) increased these to 3400 Mg a^{-1} to match observed TGM after adding Hg^0 dry deposition to the model. Our $Hg + Br$ model matches observed TGM with smaller emissions because oxidation is slower, resulting in a longer atmospheric lifetime for mercury. Our $Hg + OH/O_3$ model achieves the same result by assuming faster reduction. Atmospheric reduction can be eliminated entirely in the $Hg + Br$ model if the oxidation kinetic coefficients are reduced within their uncertainty, as described in Sect. 3.6.

Land in the model emits 1200 Mg a^{-1} from soils plus 260 Mg a^{-1} from rapid photoreduction of Hg^{II} deposited to vegetation and 260 Mg a^{-1} from snow. Even though we eliminated mercury evapotranspiration, the total land emissions are unchanged from Selin et al. (2008) because of the constraint from preindustrial steady state. Mason (2009) extrapolated field flux measurements to estimate that terrestrial ecosystems emit 1650 Mg a^{-1} (range 860–3800 Mg a^{-1}) including primary geogenic sources but excluding biomass burning. In our model the corresponding emission is 2200 Mg a^{-1}, well within that range.

Most atmospheric mercury is removed as Hg^{II} (5100 Mg a^{-1}) with the spatial pattern shown in Fig. 13. Wet deposition accounts for 3100 Mg a^{-1} and dry deposition for 800 Mg a^{-1}. Sea-salt particles take up an additional 1200 Mg a^{-1} and this accounts for 35% of Hg^{II} deposition to the ocean. Global Hg^0 dry deposition is 3200 Mg a^{-1}, but emissions offset this so that oceans and soils everywhere are net sources of atmospheric Hg^0. After accounting for all mercury species, the deep ocean in the model sequesters 1600 Mg a^{-1} from the atmosphere, similar to the previous GEOS-Chem model version (2100 Mg a^{-1}) (Selin et al., 2008).

The $Hg + OH/O_3$ model generates a very different Hg^{II} deposition pattern from the $Hg + Br$ model, except for close
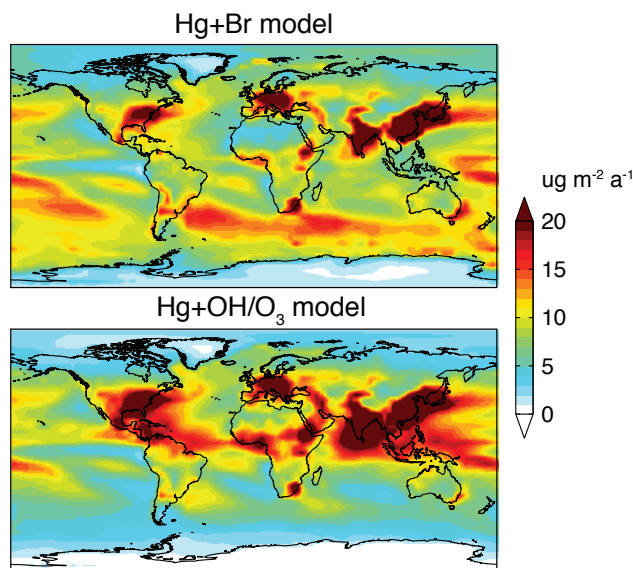

Fig. 13. Annual deposition fluxes of Hg^{II} plus Hg_P in the $Hg + Br$ and $Hg + OH/O_3$ models. Both models have 5100 Mg a^{-1} total deposition.

to Hg^{II} sources, as seen in Fig. 13. With the $Hg + OH/O_3$ oxidation mechanism, deposition is largest in the tropics where [OH] is greatest and deep convective rain occurs frequently. The $Hg + Br$ model has greater Hg^{II} deposition in the Southern Hemisphere due to the oxidation differences seen in Fig. 3. Despite these large-scale differences, both oxidation mechanisms predict similar wet deposition at monitoring sites in North America and Europe because of the anthropogenic influence (see Sect. 3.4). Figure 13 implies that wet deposition measurements in the tropics and Southern Hemisphere could distinguish between oxidation mechanisms. Furthermore, the $Hg + Br$ model suggests that mercury inputs to Southern Ocean ecosystems may be much greater than previously thought.

5 Conclusions

We have added Hg^0 oxidation by gas-phase bromine atoms to a global 3-D atmospheric model (GEOS-Chem) to test whether this reaction is consistent with the observed patterns of atmospheric mercury concentration and deposition. We compare the model performance with Br as the sole oxidant ("$Hg + Br$ model") against a model in which OH and ozone are the only oxidants ("$Hg + OH/O_3$ model"). While both oxidation mechanisms, and possibly others, may operate together in the real atmosphere, these idealized simulations enable us to explore the constraints that observations place on the atmospheric chemistry of mercury.

Total mercury emissions in the model are 8300 Mg a^{-1}, including 2050 Mg a^{-1} from anthropogenic sources. A new

snowpack reservoir stores deposited mercury and reemits it under sunlight at a temperature-dependent rate. The seasonal cycle of Arctic Hg^0 implies that 60% of mercury deposited to snow is eventually reemitted while the remainder ($60 \, Mg \, a^{-1}$) transfers to the ocean and soils.

$Hg + Br$ kinetics here follow Goodsite et al. (2004) and Donohoue et al. (2006), while $Hg + OH/O_3$ kinetics are identical to Selin et al. (2008). Global bromine distributions derive from tropospheric and stratospheric chemistry models, which are constrained by precursor gas measurements. We also specify BrO concentrations in the marine and polar springtime boundary layer based on observations. Hg^0 has a 6 month chemical lifetime in the $Hg + Br$ model and a 3.7 month lifetime in the $Hg + OH/O_3$ model. Matching atmospheric observations with the imposed anthropogenic emission inventory requires an atmospheric lifetime of 7.3 months for TGM, which we achieve by invoking photochemical reduction of Hg^{II} in clouds (at a faster rate in the $Hg + OH/O_3$ model). This reduction would be unnecessary in the $Hg + Br$ model if we decreased the overall Hg^0 oxidation rate by 60%, which is within the uncertainty of the $HgBr + X + M$ reaction step.

The $Hg + Br$ and $Hg + OH/O_3$ models both provide unbiased simulations of TGM surface concentrations and their spatial variance. In particular, the $Hg + Br$ model reproduces the interhemispheric gradient of TGM, which contradicts an earlier study (Seigneur and Lohman, 2008). Observed seasonal cycles of TGM at mid-latitudes are also consistent with both models. However, only the $Hg + Br$ model reproduces the spring depletion and summer rebound observed at polar sites. The $Hg + Br$ model also provides a better simulation of Hg^0 oxidation during subsidence events over Antarctica.

Wet deposition flux patterns of mercury observed over Europe and North America are generally reproduced in the model. Simulated deposition in the Northeast US in winter is too high regardless of oxidant, which could reflect excessive scavenging by snow, reduction of Hg^{II} in power plant plumes, or speciation error in the emission inventory. The Southeast US summer maximum in mercury wet deposition is better simulated by the $Hg + OH/O_3$ model, where it reflects scavenging of Hg^{II} from the free troposphere by deep convection.

Vertical profiles from CARIBIC, INTEX-B, and ARCTAS aircraft show uniform concentrations in the troposphere and declines above the tropopause. We reproduce these features in the $Hg + Br$ model except in Arctic spring where the observed stratospheric depletion is strongest. Neither Br nor BrO can explain the extreme stratospheric Hg^0 depletion in Arctic spring and the $Hg + OH/O_3$ model does no better. We suggest that Cl, Cl_2, or BrCl might be important in the springtime stratosphere, and estimate that the required concentrations are within the range of ClO observations.

Two major effects of using Br as the Hg^0 oxidant instead of OH and ozone are to lower Hg^0 concentrations in the Southern Hemisphere and to increase mercury deposition to

the Southern Ocean. The $Hg + OH/O_3$ model, in contrast, has peak deposition in the tropics. Mercury concentration and deposition data in the tropics and southern mid-latitudes would be necessary to test these patterns.

Our results show that gas-phase bromine is viable as the main global oxidant for Hg^0, producing a TGM lifetime and distribution consistent with nearly all available observations. Most of the oxidation occurs in the free troposphere where Br concentrations are constrained by bromocarbon measurements. We also find that atmospheric reduction of Hg^{II} may not be necessary to match observed Hg^0 concentrations if we decrease Hg^0 oxidation kinetics within its uncertainties.

References

Ababneh, F. A., Scott, S. L., Al-Reasi, H. A., and Lean, D. R. S.: Photochemical reduction and reoxidation of aqueous mercuric chloride in the presence of ferrioxalate and air, Sci. Total Environ., 367, 831–839, doi:10.1016/j.scitotenv.2006.02.018, 2006.

Ariya, P. A., Khalizov, A., and Gidas, A.: Reactions of gaseous mercury with atomic and molecular halogens: Kinetics, product studies, and atmospheric implications, J. Phys. Chem. A, 106, 7310–7320, doi:10.1021/jp020719o, 2002.

Ariya, P., Dastoor, A., Amyot, M., Schroeder, W., Barrie, L., Anlauf, K., Raofie, F., Ryzhkov, A., Davignon, D., Lalonde, J., and Steffen, A.: The Arctic: a sink for mercury, Tellus B, 56, 397–403, 2004.

Ariya, P. A., Skov, H., Grage, M. M. L., and Goodsite, M. E.: Gaseous elemental mercury in the ambient atmosphere: Review of the application of theoretical calculations and experimental studies for determination of reaction coefficients and mechanisms with halogens and other reactants, Adv. Quantum. Chem., 55, 43–55, doi:10.1016/S0065-3276(07)00204-3, 2008.

Ariya, P., Peterson, K., Snider, G., and Amyot, M.: Mercury chemical transformation in the gas, aqueous and heterogeneous phases: state-of-the-art science and uncertainties, in: Mercury Fate and Transport in the Global Atmosphere, edited by: Pirrone, N. and Mason, R. P., Springer, 2009.

Aspmo, K. and Berg, T.: "Long-term" Antarctic measurements of atmospheric mercury, in: 9th International Conference on Mercury as a Global Pollutant, Guiyang, China, 2009.

Balabanov, N., Shepler, B., and Peterson, K.: Accurate global potential energy surface and reaction dynamics for the

ground state of HgBr$_2$, J. Phys. Chem. A, 109, 8765–8773, doi:10.1021/jp0534151, 2005.

Bergan, T. and Rodhe, H.: Oxidation of elemental mercury in the atmosphere; Constraints imposed by global scale modelling, J. Atmos. Chem., 40, 191–212, 2001.

Brooks, S., Saiz-Lopez, A., Skov, H., Lindberg, S., Plane, J., and Goodsite, M.: The mass balance of mercury in the spring-time Arctic environment, Geophys. Res. Lett., 33, L13812, doi:10.1029/2005GL025525, 2006.

Brooks, S., Arimoto, R., Lindberg, S., and Southworth, G.: Antarctic polar plateau snow surface conversion of deposited oxidized mercury to gaseous elemental mercury with fractional long-term burial, Atmos. Environ., 42, 2877–2884, doi:10.1016/j.atmosenv.2007.05.029, 2008.

Bullock, O. R., Atkinson, D., Braverman, T., Civerolo, K., Dastoor, A., Davignon, D., Ku, J.-Y., Lohman, K., Myers, T. C., Park, R. J., Seigneur, C., Selin, N. E., Sistla, G., and Vijayaraghavan, K.: An analysis of simulated wet deposition of mercury from the North American Mercury Model Intercomparison Study, J. Geophys. Res., 114, D08301, doi:10.1029/2008JD011224, 2009.

Burrows, J., Weber, M., Buchwitz, M., Rozanov, V., Ladstatter-Weissenmayer, A., Richter, A., DeBeek, R., Hoogen, R., Bramstedt, K., Eichmann, K., and Eisinger, M.: The global ozone monitoring experiment (GOME): Mission concept and first scientific results, J. Atmos. Sci., 56, 151–175, 1999.

Butler, T. J., Cohen, M. D., Vermeylen, F. M., Likens, G. E., Schmeltz, D., and Artz, R. S.: Regional precipitation mercury trends in the eastern USA, 1998–2005: Declines in the Northeast and Midwest, no trend in the Southeast, Atmos. Environ., 42, 1582–1592, doi:10.1016/j.atmosenv.2007.10.084, 2008.

Caldwell, C., Swartzendruber, P., and Prestbo, E.: Concentration and dry deposition of mercury species in arid south central New Mexico (2001–2002), Environ. Sci. Technol., 40, 7535–7540, 2006.

Calvert, J. and Lindberg, S.: Mechanisms of mercury removal by O$_3$ and OH in the atmosphere, Atmos. Environ., 39, 3355–3367, doi:10.1016/j.atmosenv.2005.01.055, 2005.

Chance, K.: Analysis of BrO measurements from the Global Ozone Monitoring Experiment, Geophys. Res. Lett., 25, 3335–3338, 1998.

Choi, H.-D., Holsen, T. M., and Hopke, P. K.: Atmospheric mercury (Hg) in the Adirondacks: Concentrations and sources, Environ. Sci. Technol., 42, 5644–5653, doi:10.1021/es7028137, 2008.

Cobbett, F. D., Steffen, A., Lawson, G., and Heyst, B. J. V.: GEM fluxes and atmospheric mercury concentrations (GEM, RGM and Hg-P) in the Canadian Arctic at Alert, Nunavut, Canada (February–June 2005), Atmos. Environ., 41, 6527–6543, doi:10.1016/j.atmosenv.2007.04.033, 2007.

Cohen, M., Artz, R., Draxler, R., Miller, P., Poissant, L., Niemi, D., Ratte, D., Deslauriers, M., Duval, R., Laurin, R., Slotnick, J., Nettesheim, T., and McDonald, J.: Modeling the atmospheric transport and deposition of mercury to the Great Lakes, Environ. Res., 95, 247–265, doi:10.1016/j.envres.2003.11.007, 2004.

Dastoor, A. P., Davignon, D., Theys, N., Roozendael, M. V., Steffen, A., and Ariya, P. A.: Modeling dynamic exchange of gaseous elemental mercury at polar sunrise, Environ. Sci. Technol., 42, 5183–5188, doi:10.1021/es800291w, 2008.

Dommergue, A., Ferrari, C., Gauchard, P., Boutron, C., Poissant, L., Pilote, M., Jitaru, P., and Adams, F.: The fate of mercury

species in a sub-Arctic snowpack during snowmelt, Geophys. Res. Lett., 30, 1621, doi:10.1029/2003GL017308, 2003.

Donohoue, D., Bauer, D., and Hynes, A.: Temperature and pressure dependent rate coefficients for the reaction of Hg with Cl and the reaction of Cl with Cl: A pulsed laser photolysis-pulsed laser induced fluorescence study, J. Phys. Chem. A, 109, 7732–7741, doi:10.1021/jp0513541, 2005.

Donohoue, D., Bauer, D., Cossairt, B., and Hynes, A.: Temperature and pressure dependent rate coefficients for the reaction of Hg with Br and the reaction of Br with Br: A pulsed laser photolysis-pulsed laser induced fluorescence study, J. Phys. Chem. A, 110, 6623–6632, doi:10.1021/jp054688j, 2006.

Douglass, A., Stolarski, R., Strahan, S., and Connell, P.: Radicals and reservoirs in the GMI chemistry and transport model: Comparison to measurements, J. Geophys. Res., 109, D16302, doi:10.1029/2004JD004632, 2004.

Douglas, T. A., Sturm, M., Simpson, W. R., Blum, J. D., Alvarez-Aviles, L., Keeler, G. J., Perovich, D. K., Biswas, A., and Johnson, K.: Influence of snow and ice crystal formation and accumulation on mercury deposition to the Arctic, Environ. Sci. Technol., 42, 1542–1551, doi:10.1021/es070502d, 2008.

Ebinghaus, R., Slemr, F., Brenninkmeijer, C. A. M., van Velthoven, P., Zahn, A., Hermann, M., O'Sullivan, D. A., and Oram, D. E.: Emissions of gaseous mercury from biomass burning in South America in 2005 observed during CARIBIC flights, Geophys. Res. Lett., 34, L08813, doi:10.1029/2006GL028866, 2007.

Edgerton, E. S., Hartsell, B. E., and Jansen, J. J.: Mercury speciation in coal-fired power plant plumes observed at three surface sites in the southeastern US, Environ. Sci. Technol., 40, 4563–4570, doi:10.1021/es0515607, 2006.

EMEP: European Monitoring and Evaluation Programme: Cooperative programme for monitoring and evaluation of the long-range transmissions of air pollutants in Europe, available at: http://tarantula.nilu.no/projects/ccc/emepdata.html, 2009.

EPA: US Environmental Protection Agency, Office of Wetlands, Oceans and Watersheds, Watershed Branch: Model-Based Analysis and Tracking of Airborne Mercury Emissions to Assist in Watershed Planning, available at: http://www.epa.gov/owow/tmdl/pdf/final300report_10072008.pdf, 2008.

Fain, X., Grangeon, S., Bahlmann, E., Fritsche, J., Obrist, D., Dommergue, A., Ferrari, C. P., Cairns, W., Ebinghaus, R., Barbante, C., Cescon, P., and Boutron, C.: Diurnal production of gaseous mercury in the alpine snowpack before snowmelt, J. Geophys. Res., 112, D21311, doi:10.1029/2007JD008520, 2007.

Faïn, X., Ferrari, C. P., Dommergue, A., Albert, M., Battle, M., Arnaud, L., Barnola, J.-M., Cairns, W., Barbante, C., and Boutron, C.: Mercury in the snow and firn at Summit Station, Central Greenland, and implications for the study of past atmospheric mercury levels, Atmos. Chem. Phys., 8, 3441–3457, doi:10.5194/acp-8-3441-2008, 2008.

Feng, J.: A size-resolved model for below-cloud scavenging of aerosols by snowfall, J. Geophys. Res., 114, D08203, doi:10.1029/2008JD011012, 2009.

Feng, X., Wang, S., Qiu, G., He, T., Li, G., Li, Z., and Shang, L.: Total gaseous mercury exchange between water and air during cloudy weather conditions over Hongfeng Reservoir, Guizhou, China, J. Geophys. Res.-Atmos., 113, D15309, doi:10.1029/2007JD009600, 2008.

Finley, B. D., Swartzendruber, P. C., and Jaffe, D. A.: Particulate

mercury emissions in regional wildfire plumes observed at the Mount Bachelor Observatory, Atmos. Environ., 43, 6074–6083, doi:10.1016/j.atmosenv.2009.08.046, 2009.

Friedli, H. R., Arellano, A. F., Cinnirella, S., and Pirrone, N.: Initial estimates of mercury emissions to the atmosphere from global biomass burning, Environ. Sci. Technol., 43, 3507–3513, 2009.

Gårdfeldt, K. and Jonsson, M.: Is bimolecular reduction of Hg(II) complexes possible in aqueous systems of environmental importance, J. Phys. Chem. A, 107, 4478–4482, doi:10.1021/jp0275342, 2003.

Goodsite, M., Plane, J., and Skov, H.: A theoretical study of the oxidation of Hg^0 to $HgBr_2$ in the troposphere, Environ. Sci. Technol., 38, 1772–1776, doi:10.1021/es034680s, 2004.

Guentzel, J., Landing, W., Gill, G., and Pollman, C.: Processes influencing rainfall deposition of mercury in Florida, Environ. Sci. Technol., 35, 863–873, doi:10.1021/es001523+, 2001.

Gusev, A., Illiyn, I., Rozovskaya, O., Shatalov, V., Sokovych, V., and Travnikov, O.: Modelling of heavy metals and persistent organic pollutants: New developments, Tech. rep., EMEP/MSC-E, 2009.

Gustin, M., Ericksen, J., Schorran, D., Johnson, D., Lindberg, S., and Coleman, J.: Application of controlled mesocosms for understanding mercury air-soil-plant exchange, Environ. Sci. Technol., 38, 6044–6050, doi:10.1021/es0487933, 2004.

Hall, B.: The gas phase oxidation of elemental mercury by ozone, Water Air Soil Poll., 80, 301–315, 1995.

Hedgecock, I. and Pirrone, N.: Mercury and photochemistry in the marine boundary layer-modelling studies suggest the in situ production of reactive gas phase mercury, Atmos. Environ., 35, 3055–3062, 2001.

Hedgecock, I., Trunfio, G., Pirrone, N., and Sprovieri, F.: Mercury chemistry in the MBL: Mediterranean case and sensitivity studies using the AMCOTS (Atmospheric Mercury Chemistry over the Sea) model, Atmos. Environ., 39, 7217–7230, 2005.

Holmes, C., Jacob, D., and Yang, X.: Global lifetime of elemental mercury against oxidation by atomic bromine in the free troposphere, Geophys. Res. Lett., 33, L20808, doi:10.1029/2006GL027176, 2006.

Holmes, C. D., Jacob, D. J., Mason, R. P., and Jaffe, D. A.: Sources and deposition of reactive gaseous mercury in the marine atmosphere, Atmos. Environ., 43, 2278–2285, doi:10.1016/j.atmosenv.2009.01.051, 2009.

Hylander, L. D. and Meili, M.: The rise and fall of mercury: converting a resource to refuse after 500 years of mining and pollution, Crit. Rev. Environ. Sci. Technol., 34, 1–36, 2005.

Hynes, A., Donohoue, D., Goodsite, M., Hedgecock, I., Pirrone, N., and Mason, R.: Our current understanding of major chemical and physical processes affecting mercury dynamics in the atmosphere and at air-water/terrestrial interfaces, in: Mercury Fate and Transport in the Global Atmosphere, edited by: Pirrone, N. and Mason, R. P., chap. 14, Springer, 2009.

Jacob, D. J., Crawford, J. H., Maring, H., Clarke, A. D., Dibb, J. E., Emmons, L. K., Ferrare, R. A., Hostetler, C. A., Russell, P. B., Singh, H. B., Thompson, A. M., Shaw, G. E., McCauley, E., Pederson, J. R., and Fisher, J. A.: The Arctic Research of the Composition of the Troposphere from Aircraft and Satellites (ARC-TAS) mission: design, execution, and first results, Atmos. Chem. Phys., 10, 5191–5212, doi:10.5194/acp-10-5191-2010, 2010.

Jaffe, D., Prestbo, E., Swartzendruber, P., Weiss-Penzias, P., Kato,

S., Takami, A., Hatakeyama, S., and Kajii, Y.: Export of atmospheric mercury from Asia, Atmos. Environ., 39, 3029–3038, doi:10.1016/j.atmosenv.2005.01.030, 2005.

Johnson, K. P., Blum, J. D., Keeler, G. J., and Douglas, T. A.: Investigation of the deposition and emission of mercury in arctic snow during an atmospheric mercury depletion event, J. Geophys. Res., 113, D17304, doi:10.1029/2008JD009893, 2008.

Kim, S., Talbot, R. W., and Mao, H.: 2009, Eos Transactions, Fall Meeting Suppl, 90, A43A–0190, 2009.

Kirk, J. L., Louis, V. L. S., and Sharp, M. J.: Rapid reduction and reemission of mercury deposited into snowpacks during atmospheric mercury depletion events at Churchill, Manitoba, Canada, Environ. Sci. Technol., 40, 7590–7596, doi:10.1021/es061299, 2006.

Lamborg, C., Rolfhus, K., Fitzgerald, W., and Kim, G.: The atmospheric cycling and air-sea exchange of mercury species in the South and equatorial Atlantic Ocean, Deep-sea Research II, 46, 957–977, 1999.

Lamborg, C., Fitzgerald, W., O'Donnell, J., and Torgersen, T.: A non-steady-state compartmental model of global-scale mercury biogeochemistry with interhemispheric atmospheric gradients, Geochim. Cosmochim. Ac., 66, 1105–1118, 2002.

Landis, M., Ryan, J., Oswald, E., Jansen, J., Monroe, L., Walters, J., Levin, L., ter Schure, A., Laudal, D., and Edgerton, E.: Plant Crist mercury plume study, in: Air Quality VII, Arlington, VA, October 27, 2009.

Laurier, F. and Mason, R.: Mercury concentration and speciation in the coastal and open ocean boundary layer, J. Geophys. Res., 112, D06302, doi:10.1029/2006JD007320, 2007.

Laurier, F., Mason, R., Whalin, L., and Kato, S.: Reactive gaseous mercury formation in the North Pacific Ocean's marine boundary layer: A potential role of halogen chemistry, J. Geophys. Res., 108, 4529, doi:10.1029/2003JD003625, 2003.

Leser, H., Honninger, G., and Platt, U.: MAX-DOAS measurements of BrO and NO_2 in the marine boundary layer, Geophys. Res. Lett., 30, 1537, doi:10.1029/2002GL015811, 2003.

Liang, Q., Stolarski, R. S., Kawa, S. R., Nielsen, J. E., Douglass, A. R., Rodriguez, J. M., Blake, D. R., Atlas, E. L., and Ott, L. E.: Finding the missing stratospheric Bry: a global modeling study of $CHBr_3$ and CH_2Br_2, Atmos. Chem. Phys., 10, 2269–2286, doi:10.5194/acp-10-2269-2010, 2010.

Lin, J.-T. and McElroy, M.: Impacts of boundary layer mixing on pollutant vertical profiles in the lower troposphere: Implications to satellite remote sensing, Atmos. Environ., 44, 1726–1739, doi:10.1016/j.atmosenv.2010.02.009, 2010.

Lin, C., Pongprueksa, P., Lindberg, S., Pehkonen, S., Byun, D., and Jang, C.: Scientific uncertainties in atmospheric mercury models I: Model science evaluation, Atmos. Environ., 40, 2911–2928, 2006.

Lindberg, S., Bullock, R., Ebinghaus, R., Engstrom, D., Feng, X., Fitzgerald, W., Pirrone, N., Prestbo, E., and Seigneur, C.: A synthesis of progress and uncertainties in attributing the sources of mercury in deposition, Ambio, 36, 19–32, 2007.

Lindqvist, O. and Rodhe, H.: Atmospheric mercury – a review, Tellus B, 37, 136–159, 1985.

Liu, H., Jacob, D., Bey, I., and Yantosca, R.: Constraints from Pb-210 and Be-7 on wet deposition and transport in a global three-dimensional chemical tracer model driven by assimilated meteorological fields, J. Geophys. Res., 106, 12109–12128, 2001.

Liu, B., Keeler, G. J., Dvonch, J. T., Barres, J. A., Lynam, M. M., Marsik, F. J., and Morgan, J. T.: Temporal variability of mercury speciation in urban air, Atmos. Environ., 41, 1911–1923, doi:10.1016/j.atmosenv.2006.10.063, 2007.

Lohman, K., Seigneur, C., Edgerton, E., and Jansen, J.: Modeling mercury in power plant plumes, Environ. Sci. Technol., 40, 3848–3854, doi:10.1021/es051556v, 2006.

Lyman, S. N. and Gustin, M. S.: Speciation of atmospheric mercury at two sites in northern Nevada, USA, Atmos. Environ., 42, 927–939, doi:10.1016/j.atmosenv.2007.10.012, 2008.

MacKenzie, D.: Seasonal variations in the mixing layer in the UTLS, in: GEOS-Chem User's Meeting, Cambridge, MA USA, 2009.

Mao, H., Talbot, R. W., Sive, B. C., Kim, S.-Y., Blake, D. R., and Weinheimer, A. J.: Arctic mercury depletion and its quantitative link with halogens, J. Atmos. Chem., in review, 2010.

Mao, J., Jacob, D. J., Evans, M. J., Olson, J. R., Ren, X., Brune, W. H., Clair, J. M. St., Crounse, J. D., Spencer, K. M., Beaver, M. R., Wennberg, P. O., Cubison, M. J., Jimenez, J. L., Fried, A., Weibring, P., Walega, J. G., Hall, S. R., Weinheimer, A. J., Cohen, R. C., Chen, G., Crawford, J. H., McNaughton, C., Clarke, A. D., Jaeglé, L., Fisher, J. A., Yantosca, R. M., Le Sager, P., and Carouge, C.: Chemistry of hydrogen oxide radicals (HO_x) in the Arctic troposphere in spring, Atmos. Chem. Phys., 10, 5823–5838, doi:10.5194/acp-10-5823-2010, 2010.

Martin, M., Pöhler, D., Seitz, K., Sinreich, R., and Platt, U.: BrO measurements over the Eastern North-Atlantic, Atmos. Chem. Phys., 9, 9545–9554, doi:10.5194/acp-9-9545-2009, 2009.

Mason, R. P.: Mercury emissions from natural processes and their importance in the global mercury cycle, in: Mercury Fate and Transport in the Global Atmosphere, edited by: Pirrone, N. and Mason, R. P., chap. 7, Springer, 2009.

Mason, R. and Sheu, G.: Role of the ocean in the global mercury cycle, Global Biogeochem. Cy., 16, 1093, doi:10.1029/2001GB001440, 2002.

Murakami, M., Kimura, T., Magono, C., and Kikuchi, K.: Observations of precipitation scavenging for water-soluble particles, J. Meteorol. Soc. Jpn., 61, 346–358, 1983.

National Atmospheric Deposition Program: Mercury Deposition Network (MDN): A NADP Network, available at: http://nadp. sws.uiuc.edu/MDN/, 2009.

Nguyen, H. T., Kim, K.-H., Kim, M.-Y., Hong, S., Youn, Y.-H., Shon, Z.-H., and Lee, J. S.: Monitoring of atmospheric mercury at a global atmospheric watch (GAW) site on An-Myun Island, Korea, Water Air Soil Poll., 185, 149–164, doi:10.1007/s11270-007-9438-5, 2007.

O'Brien, L. M., Harris, N. R. P., Robinson, A. D., Gostlow, B., Warwick, N., Yang, X., and Pyle, J. A.: Bromocarbons in the tropical marine boundary layer at the Cape Verde Observatory - measurements and modelling, Atmos. Chem. Phys., 9, 9083–9099, doi:10.5194/acp-9-9083-2009, 2009.

Pacyna, E. G., Pacyna, J. M., Steenhuisen, F., and Wilson, S.: Global anthropogenic mercury emission inventory for 2000, Atmos. Environ., 40, 4048–4063, doi:10.1016/j.atmosenv.2006.03.041, 2006.

Pacyna, J. M., Pacyna, E. G., and Aas, W.: Changes of emissions and atmospheric deposition of mercury, lead, and cadmium, Atmos. Environ., 43, 117–127, doi:10.1016/j.atmosenv.2008.09.066, 2009.

Pacyna, E. G., Pacyna, J. M., Sundseth, K., Munthe, J., Kindbom, K., Wilson, S., Steenhuisen, F., and Maxson, P.: Global emission of mercury to the atmosphere from anthropogenic sources in 2005 and projections to 2020, Atmos. Environ., 44, 2487–2499, doi:10.1016/j.atmosenv.2009.06.009, 2010.

Park, R., Jacob, D., Field, B., Yantosca, R., and Chin, M.: Natural and transboundary pollution influences on sulfate-nitrate-ammonium aerosols in the United States: implications for policy, J. Geophys. Res., 109, D15204, doi:10.1029/2003JD004473, 2004.

Parrella, J. P., Evans, M. J., Jacob, D. J., Liang, Q., Mickley, L. J., Miller, B., Pyle, J. A., and Yang, X.: Effect of bromine chemistry on natural tropospheric ozone: improved simulation of concentrations from the turn of the 20th century, Nature, in preparation, 2010.

Pehkonen, S. and Lin, C.: Aqueous photochemistry of mercury with organic acids, J. Air Waste Manage., 48, 144–150, 1998.

Petersen, G., Bloxam, R., Wong, S., Munthe, J., Kruger, O., Schmolke, S., and Kumar, A.: A comprehensive Eulerian modelling framework for airborne mercury species: model development and applications in Europe, Atmos. Environ., 35, 3063–3074, 2001.

Pirrone, N., Cinnirella, S., Feng, X., Finkelman, R. B., Friedli, H. R., Leaner, J., Mason, R., Mukherjee, A. B., Stracher, G. B., Streets, D. G., and Telmer, K.: Global mercury emissions to the atmosphere from anthropogenic and natural sources, Atmos. Chem. Phys., 10, 5951–5964, doi:10.5194/acp-10-5951-2010, 2010.

Platt, U. and Janssen, C.: Observation and role of the free radicals NO_3, ClO, BrO and IO in the troposphere, Faraday Discuss., 100, 175–198, 1995.

Pongprueksa, P., Lin, C.-J., Lindberg, S. E., Jang, C., Braverman, T., Bullock, O. R., Ho, T. C., and Wei Chu, H.: Scientific uncertainties in atmospheric mercury models III: Boundary and initial conditions, model grid resolution, and Hg(II) reduction mechanism, Atmos. Environ., 42, 1828–1845, doi:10.1016/j.atmosenv.2007.11.020, 2008.

Prestbo, E. M. and Gay, D. A.: Wet deposition of mercury in the US and Canada, 1996–2005: Results and analysis of the NADP mercury deposition network (MDN), Atmos. Environ., 43, 4223–4233, doi:10.1016/j.atmosenv.2009.05.028, 2009.

Pruppacher, H. R. and Jaenicke, R.: The processing of water-vapor and aerosols by atmospheric clouds, a global estimate, Atmos. Res., 38, 283–295, 1995.

Pszenny, A. A. P., Moldanová, J., Keene, W. C., Sander, R., Maben, J. R., Martinez, M., Crutzen, P. J., Perner, D., and Prinn, R. G.: Halogen cycling and aerosol pH in the Hawaiian marine boundary layer, Atmos. Chem. Phys., 4, 147–168, doi:10.5194/acp-4-147-2004, 2004.

Pundt, I., Pommereau, J., Chipperfield, M., Roozendael, M. V., and Goutail, F.: Climatology of the stratospheric BrO vertical distribution by balloon-borne UV-visible spectrometry, J. Geophys. Res., 107, 4806, doi:10.1029/2002JD002230, 2002.

Raofie, F. and Ariya, P.: Product study of the gas-phase BrO-initiated oxidation of Hg^0: evidence for stable Hg1+ compounds, Environ. Sci. Technol., 38, 4319–4326, doi:10.1021/es035339a, 2004.

Richter, A., Wittrock, F., Ladstatter-Weissenmayer, A., and Burrows, J.: GOME measurements of stratospheric and tropospheric

BrO, Adv. Space Res., 29, 1667–1672, 2002.

Rutter, A. P. and Schauer, J. J.: The impact of aerosol composition on the particle to gas partitioning of reactive mercury, Environ. Sci. Technol., 41, 3934–3939, doi:10.1021/es062439i, 2007a.

Rutter, A. P. and Schauer, J. J.: The effect of temperature on the gas-particle partitioning of reactive mercury in atmospheric aerosols, Atmos. Environ., 41, 8647–8657, doi:10.1016/j.atmosenv.2007.07.024, 2007b.

Saiz-Lopez, A., Plane, J., and Shillito, J.: Bromine oxide in the mid-latitude marine boundary layer, Geophys. Res. Lett., 31, L03111, doi:10.1029/2003GL018956, 2004.

Sakata, M. and Asakura, K.: Estimating contribution of precipitation scavenging of atmospheric particulate mercury to mercury wet deposition in Japan, Atmos. Environ., 41, 1669–1680, doi:10.1016/j.atmosenv.2006.10.031, 2007.

Salawitch, R., Weisenstein, D., Kovalenko, L., Sioris, C., Wennberg, P., Chance, K., Ko, M., and McLinden, C.: Sensitivity of ozone to bromine in the lower stratosphere, Geophys. Res. Lett., 32, L05811, doi:10.1029/2004GL021504, 2005.

Salawitch, R. J., Canty, T. P., Kurosu, T. P., Chance, K., Liang, Q., da Silva, A., Pawson, S., Nielsen, J. E., Rodriguez, J. M., Bhartia, P. K., Liu, X., Huey, L. G., Liao, J., Stickel, R. E., Tanner, D., Dibb, J. E., Simpson, W. R., Donohoue, D., Weinheimer, A. J., Flock, F. M., Knapp, D. J., Dmontzka, D. D., Neuman, J., Nowak, J. B., Ryerson, T. B., Oltmans, S., Blake, D. R., Atlas, E. L., Kinnison, D. E., Tilmes, S., Pan, L., Hendrick, F., Van Roozendael, M., Kreher, K., Johnston, P. V., Gao, R. S., Bui, T. P., Chen, G., Pierce, R., Crawford, J. H., and Jacob, D. J.: A new interpretation of total column BrO during Arctic spring, Geophys. Res. Lett., 37, L21805, doi:10.1029/2010GL043798, 2010.

Sander, S. P., Ravishankara, A. R., Golden, D. M., Kolb, C. E., Kurylo, M. J., Molina, M. J., Moortgat, G. K., Finlayson-Pitts, B. J., Wine, P. H., and Huie, R. E.: Chemical Kinetics and Photochemical Data for Use in Atmospheric Studies: Evaluation Number 15, Tech. rep., NASA Panel for Data Evaluation, available at: http://jpldataeval.jpl.nasa.gov/, 2006.

Seigneur, C. and Lohman, K.: Effect of bromine chemistry on the atmospheric mercury cycle, J. Geophys. Res., 113, D23309, doi:10.1029/2008JD010262, 2008.

Seigneur, C., Vijayaraghavan, K., and Lohman, K.: Atmospheric mercury chemistry: Sensitivity of global model simulations to chemical reactions, J. Geophys. Res., 111, D22306, doi:10.1029/2005JD006780, 2006.

Selin, N. E. and Jacob, D. J.: Seasonal and spatial patterns of mercury wet deposition in the United States: Constraints on the contribution from North American anthropogenic sources, Atmos. Environ., 42, 5193–5204, doi:10.1016/j.atmosenv.2008.02.069, 2008.

Selin, N. E., Jacob, D. J., Park, R. J., Yantosca, R. M., Strode, S., Jaeglé, L., and Jaffe, D.: Chemical cycling and deposition of atmospheric mercury: Global constraints from observations, J. Geophys. Res., 112, 1–14, doi:10.1029/2006JD007450, 2007.

Selin, N. E., Jacob, D. J., Yantosca, R. M., Strode, S., Jaeglé, L., and Sunderland, E. M.: Global 3-D land-ocean-atmosphere model for mercury: Present-day versus preindustrial cycles and anthropogenic enrichment factors for deposition, Global Biogeochem. Cyc., 22, 1–13, doi:10.1029/2007GB003040, 2008.

Shia, R., Seigneur, C., Pai, P., Ko, M., and Sze, N.: Global sim-ulation of atmospheric mercury concentrations and deposition fluxes, J. Geophys. Res., 104, 23747–23760, 1999.

Si, L. and Ariya, P. A.: Reduction of oxidized mercury species by dicarboxylic acids (C-2-C-4): Kinetic and product studies, Environ. Sci. Technol., 42, 5150–5155, doi:10.1021/es800552z, 2008.

Sigler, J. M., Mao, H., and Talbot, R.: Gaseous elemental and reactive mercury in Southern New Hampshire, Atmos. Chem. Phys., 9, 1929–1942, doi:10.5194/acp-9-1929-2009, 2009.

Simpson, W. R., von Glasow, R., Riedel, K., Anderson, P., Ariya, P., Bottenheim, J., Burrows, J., Carpenter, L. J., Frieß, U., Goodsite, M. E., Heard, D., Hutterli, M., Jacobi, H.-W., Kaleschke, L., Neff, B., Plane, J., Platt, U., Richter, A., Roscoe, H., Sander, R., Shepson, P., Sodeau, J., Steffen, A., Wagner, T., and Wolff, E.: Halogens and their role in polar boundary-layer ozone depletion, Atmos. Chem. Phys., 7, 4375-4-418, doi:10.5194/acp-7-4375-2007, 2007.

Singh, H. B., Brune, W. H., Crawford, J. H., Flocke, F., and Jacob, D. J.: Chemistry and transport of pollution over the Gulf of Mexico and the Pacific: spring 2006 INTEX-B campaign overview and first results, Atmos. Chem. Phys., 9, 2301–2318, doi:10.5194/acp-9-2301-2009, 2009.

Sinnhuber, B., Rozanov, A., Sheode, N., Afe, O., Richter, A., Sinnhuber, M., Wittrock, F., Burrows, J., Stiller, G., von Clarmann, T., and Linden, A.: Global observations of stratospheric bromine monoxide from SCIAMACHY, Geophys. Res. Lett., 32, L20810, doi:10.1029/2005GL023839, 2005.

Sioris, C. E., Kovalenko, L. J., McLinden, C. A., Salawitch, R. J., Roozendael, M. V., Goutail, F., Dorf, M., Pfeilsticker, K., Chance, K., von Savigny, C., Liu, X., Kurosu, T. P., Pommereau, J. P., Boesch, H., and Frerick, J.: Latitudinal and vertical distribution of bromine monoxide in the lower stratosphere from Scanning Imaging Absorption Spectrometer for Atmospheric Chartography limb scattering measurements, J. Geophys. Res., 111, D14301, doi:10.1029/2005JD006479, 2006.

Slemr, F., Brunke, E. G., Labuschagne, C., and Ebinghaus, R.: Total gaseous mercury concentrations at the Cape Point GAW station and their seasonality, Geophys. Res. Lett., 35, L11807, doi:10.1029/2008GL033741, 2008.

Slemr, F., Ebinghaus, R., Brenninkmeijer, C. A. M., Hermann, M., Kock, H. H., Martinsson, B. G., Schuck, T., Sprung, D., van Velthoven, P., Zahn, A., and Ziereis, H.: Gaseous mercury distribution in the upper troposphere and lower stratosphere observed onboard the CARIBIC passenger aircraft, Atmos. Chem. Phys., 9, 1957–1969, doi:10.5194/acp-9-1957-2009, 2009.

Slemr, F., Brunke, E.-G., Ebinghaus, R., Kuss, J., and Edgerton, E. S.: Worldwide trend of atmospheric mercury since 1995, in preparation, 2010.

Snider, G., Raofie, F., and Ariya, P.: Effects of relative humidity and CO(g) on the O_3-initiated oxidation reaction of Hg^0: kinetic and product studies, Phys. Chem. Chem. Phys., 10, 5616–5623, 2008.

Soerensen, A. L., Skov, H., Jacob, D. J., Soerensen, B. T., and Johnson, M. S.: Global concentrations of gaseous elemental mercury and reactive gaseous mercury in the marine boundary layer, Environ. Sci. Technol., 44, 425–427, 2010a.

Soerensen, A. L., Sunderland, E. M., Holmes, C. D., Jacob, D. J., Yantosca, R. M., Skov, H., Christensen, J. J., and Mason, R. P.: An improved global model for air-sea exchange of mercury: high

concentrations over the North Atlantic, Environ. Sci. Technol., 44, 8574–8580, doi:10.1021/es102032g, 2010b.

Sommar, J., Gardfeldt, K., Stromberg, D., and Feng, X.: A kinetic study of the gas-phase reaction between the hydroxyl radical and atomic mercury, Atmos. Environ., 35, 3049–3054, 2001.

Sprovieri, F., Pirrone, N., Hedgecock, I., Landis, M., and Stevens, R.: Intensive atmospheric mercury measurements at Terra Nova Bay in Antarctica during November and December 2000, J Geophys Res, 107, 4722, doi:10.1029/2002JD002057, 2002.

Stamenkovic, J., Lyman, S., and Gustin, M. S.: Seasonal and diel variation of atmospheric mercury concentrations in the Reno (Nevada, USA) airshed, Atmos. Environ., 41, 6662–6672, doi:10.1016/j.atmosenv.2007.04.015, 2007.

Steffen, A., Schroeder, W., Macdonald, R., Poissant, L., and Konoplev, A.: Mercury in the Arctic atmosphere: An analysis of eight years of measurements of GEM at Alert (Canada) and a comparison with observations at Amderma (Russia) and Kuujjuarapik (Canada), Sci. Total. Environ., 342, 185–198, 2005.

Steffen, A., Douglas, T., Amyot, M., Ariya, P., Aspmo, K., Berg, T., Bottenheim, J., Brooks, S., Cobbett, F., Dastoor, A., Dommergue, A., Ebinghaus, R., Ferrari, C., Gardfeldt, K., Goodsite, M. E., Lean, D., Poulain, A. J., Scherz, C., Skov, H., Sommar, J., and Temme, C.: A synthesis of atmospheric mercury depletion event chemistry in the atmosphere and snow, Atmos. Chem. Phys., 8, 1445–1482, doi:10.5194/acp-8-1445-2008, 2008.

Strahan, S. E., Duncan, B. N., and Hoor, P.: Observationally derived transport diagnostics for the lowermost stratosphere and their application to the GMI chemistry and transport model, Atmos. Chem. Phys., 7, 2435–2445, doi:10.5194/acp-7-2435-2007, 2007.

Streets, D., Zhang, Q., and Wu, Y.: Projections of global mercury emissions in 2050, Environ. Sci. Technol., 43, 2983–2988, doi:10.1021/es802474j, 2009.

Strode, S. A., Jaegle, L., Selin, N. E., Jacob, D. J., Park, R. J., Yantosca, R. M., Mason, R. P., and Slemr, F.: Air-sea exchange in the global mercury cycle, Global Biogeochem. Cy., 21, GB1017, doi:10.1029/2006GB002766, 2007.

Sunderland, E. M. and Mason, R. P.: Human impacts on open ocean mercury concentrations, Global Biogeochem. Cy., 21, GB4022, doi:10.1029/2006GB002876, 2007.

Swartzendruber, P. C., Chand, D., Jaffe, D. A., Smith, J., Reidmiller, D., Gratz, L., Keeler, J., Strode, S., Jaegle, L., and Talbot, R.: Vertical distribution of mercury, CO, ozone, and aerosol scattering coefficient in the Pacific Northwest during the spring 2006 INTEX-B campaign, J. Geophys. Res., 113, D10305, doi:10.1029/2007JD009579, 2008.

Talbot, R., Mao, H., Scheuer, E., Dibb, J., and Avery, M.: Total depletion of Hg^0 in the upper troposphere-lower stratosphere, Geophys. Res. Lett., 34, L23804, doi:10.1029/2007GL031366, 2007.

Talbot, R., Mao, H., Scheuer, E., Dibb, J., Avery, M., Browell, E., Sachse, G., Vay, S., Blake, D., Huey, G., and Fuelberg, H.: Factors influencing the large-scale distribution of Hg^0 in the Mexico City area and over the North Pacific, Atmos. Chem. Phys., 8, 2103-2114, doi:10.5194/acp-8-2103-2008, 2008.

Talbot, R. W. and Mao, H.: Boreal forest fires and pyrocumulonimbus convection as a source of Hg(0) to the troposphere, Eos Transactions, Fall Meeting Suppl, 90, A43A–0228, 2009.

Telmer, K. H. and Veiga, M. M.: World emissions of mercury from artisanal and small scale gold mining, in: Mercury Fate and Transport in the Global Atmosphere, edited by: Pirrone, N. and Mason, R. P., chap. 6, Springer, 2009.

Temme, C., Einax, J., Ebinghaus, R., and Schroeder, W.: Measurements of atmospheric mercury species at a coastal site in the Antarctic and over the South Atlantic Ocean during polar summer, Environ. Sci. Technol., 37, 22–31, 2003.

Temme, C., Blanchard, P., Steffen, A., Banic, C., Beauchamp, S., Poissant, L., Tordon, R., and Wiens, B.: Trend, seasonal and multivariate analysis study of total gaseous mercury data from the Canadian atmospheric mercury measurement network (CAMNet), Atmos. Environ., 41, 5423–5441, doi:10.1016/j.atmosenv.2007.02.021, 2007.

Thornton, B., Toohey, D., Avallone, L., Harder, H., Martinez, M., Simpas, J., Brune, W., and Avery, M.: In situ observations of ClO near the winter polar tropopause, J. Geophys. Res., 108, 8333, doi:10.1029/2002JD002839, 2003.

Valente, R., Shea, C., Humes, K., and Tanner, R.: Atmospheric mercury in the Great Smoky Mountains compared to regional and global levels, Atmos. Environ., 41, 1861–1873, 2007.

Van Loon, L., Mader, E., and Scott, S.: Reduction of the aqueous mercuric ion by sulfite: UV spectrum of $HgSO_3$ and its intramolecular redox reaction, J. Phys. Chem. A, 104, 1621–1626, 2000.

Van Roozendael, M., Wagner, T., Richter, A., Pundt, I., Arlander, D., Burrows, J., Chipperfield, M., Fayt, C., Johnston, P., Lambert, J., Kreher, K., Pfeilsticker, K., Platt, U., Pommereau, J., Sinnhuber, B., Tornkvist, K., and Wittrock, F.: Intercomparison of BrO measurements from ERS-2 GOME, ground-based and balloon platforms, Adv. Space Res., 29, 1661–1666, 2002.

Vijayaraghavan, K., Karamchandani, P., Seigneur, C., Balmori, R., and Chen, S.-Y.: Plume-in-grid modeling of atmospheric mercury, J. Geophys. Res., 113, D24305, doi:10.1029/2008JD010580, 2008.

von Glasow, R., Sander, R., Bott, A., and Crutzen, P.: Modeling halogen chemistry in the marine boundary layer – 1. Cloud-free MBL, J. Geophys. Res., 107, 4341, doi:10.1029/2001JD000942, 2002.

von Glasow, R., von Kuhlmann, R., Lawrence, M. G., Platt, U., and Crutzen, P. J.: Impact of reactive bromine chemistry in the troposphere, Atmos. Chem. Phys., 4, 2481–2497, doi:10.5194/acp-4-2481-2004, 2004.

Wan, Q., Feng, X., Lu, J., Zheng, W., Song, X., Han, S., and Xu, H.: Atmospheric mercury in Changbai Mountain area, northeastern China I. The seasonal distribution pattern of total gaseous mercury and its potential sources, Environ. Res., 109, 201–206, doi:10.1016/j.envres.2008.12.001, 2009.

Wangberg, I., Munthe, J., Berg, T., Ebinghaus, R., Kock, H. H., Temme, C., Bieber, E., Spain, T. G., and Stolk, A.: Trends in air concentration and deposition of mercury in the coastal environment of the North Sea Area, Atmos. Environ., 41, 2612–2619, doi:10.1016/j.atmosenv.2006.11.024, 2007.

Warwick, N., Pyle, J., Carver, G., Yang, X., Savage, N., O'Connor, F., and Cox, R.: Global modeling of biogenic bromocarbons, J. Geophys. Res., 111, D24305, doi:10.1029/2006JD007264, 2007.

Weiss-Penzias, P., Jaffe, D., Swartzendruber, P., Hafner, W., Chand, D., and Prestbo, E.: Quantifying Asian and biomass burning sources of mercury using the Hg/CO ratio in pollution plumes observed at the Mount Bachelor Observatory, Atmos. Environ.,

41, 4366–4379, doi:10.1016/j.atmosenv.2007.01.058, 2007.

Weiss-Penzias, P., Gustin, M. S., and Lyman, S. N.: Observations of speciated atmospheric mercury at three sites in Nevada: Evidence for a free tropospheric source of reactive gaseous mercury, J. Geophys. Res., 114, D14302, doi:10.1029/2008JD011607, 2009.

Wesely, M.: Parameterization of surface resistances to gaseous dry deposition in regional-scale numerical models, Atmos. Environ., 23, 1293–1304, 1989.

WMO: Scientific Assessment of Ozone Depletion: 2006, Tech. Rep. 50, Global Ozone Research and Monitoring Project, Geneva, Switzerland, 2007.

Xie, Z.-Q., Sander, R., Pöschl, U., and Slemr, F.: Simulation of atmospheric mercury depletion events (AMDEs) during polar springtime using the MECCA box model, Atmos. Chem. Phys., 8, 7165–7180, doi:10.5194/acp-8-7165-2008, 2008.

Yang, X., Cox, R., Warwick, N., Pyle, J., Carver, G., O'Connor, F., and Savage, N.: Tropospheric bromine chemistry and its impacts on ozone: A model study, J. Geophys. Res., 110, D23311, doi:10.1029/2005JD006244, 2005.

Yang, X., Pyle, J. A., Cox, R. A., Theys, N., and Van Roozendael, M.: Snow-sourced bromine and its implications for polar tropospheric ozone, Atmos. Chem. Phys., 10, 7763–7773, doi:10.5194/acp-10-7763-2010, 2010.

Yatavelli, R. L. N., Fahrni, J. K., Kim, M., Crist, K. C., Vickers, C. D., Winter, S. E., and Connell, D. P.: Mercury, PM2.5 and gaseous co-pollutants in the Ohio River Valley region: Preliminary results from the Athens supersite, Atmos. Environ., 40, 6650–6665, doi:10.1016/j.atmosenv.2006.05.072, 2006.

Zhang, H., Lindberg, S., Marsik, F., and Keeler, G.: Mercury air/surface exchange kinetics of background soils of the Tahquamenon River watershed in the Michigan Upper Peninsula, Water Air Soil Poll., 126, 151–169, 2001.